Technical University of Munich

DLR Deutsches Zentrum für Luft- und Raumfahrt
German Aerospace Center

Reactor for Plasma Processing of Aerodynamically Levitated Samples

Reaktor für die Plasmabearbeitung von aerodynamisch levitierenden Proben

Master's Thesis

M.Sc. Aerospace Engineering

Author:	Mert Mustu
Matriculation Number:	03765843
Supervisor:	Prof. Dr. Rudolf Neu
	Dr. Hubertus Thomas
	Dr. Mikhail Pustylnik

2025-09-30

Statutory Declaration

I, Mert Mustu, declare on oath towards the Institute of Plasma Component Interaction of Technical University of Munich and the Institute of Frontier Materials on Earth and in Space of DLR, that I have prepared the present Master's Thesis independently and with the aid of nothing but the resources listed in the bibliography.

This thesis has neither as-is nor similarly been submitted to any other university.

Munich, 2025-09-30

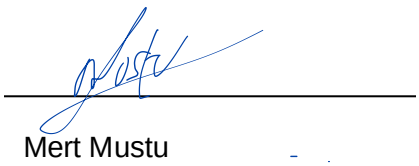

Mert Mustu

Abstract

In materials research, aerodynamic levitation and dielectric barrier discharge (DBD) plasma jets have already been applied to study material properties under realistic conditions. The combination of these two methods, however, opens new opportunities for analyzing chemical surface reactions in high-temperature resistant materials. The objective of this thesis was therefore the development of a reactor that couples a levitator module with a DBD plasma system, enabling container-free processing with direct plasma interaction.

The reactor avoids disturbances caused by vessel walls and allows independent temperature control of the sample. This is achieved through the combined use of a CO_2 laser for targeted heating and a cold atmospheric pressure plasma for chemical activation. An integrated diagnostic system provides continuous observation and evaluation of the samples during operation, while design measures for electrical insulation and thermal stabilization ensure reliable performance.

The results demonstrate the technical feasibility of combining aerodynamic levitation with a DBD plasma jet. Stable levitation with simultaneous plasma exposure was successfully achieved, establishing a new experimental platform for studying oxidation and reduction processes. This reactor provides the basis for more precise material characterization under realistic process conditions and opens perspectives for further studies on surface reaction kinetics and time-resolved diagnostics.

Kurzfassung

In der Materialforschung werden aerodynamische Levitation und dielektrische Barriereentladungs-Plasmajets bereits eingesetzt, um Materialeigenschaften unter realitätsnahen Bedingungen zu untersuchen. Die Kombination beider Methoden eröffnet jedoch neue Möglichkeiten zur Analyse chemischer Oberflächenreaktionen an hochtemperaturbeständigen Materialien. Ziel dieser Arbeit war die Entwicklung eines Reaktors, der ein Levitatormodul mit einem DBD-Plasmasystem koppelt und dadurch containerfreie Prozesse mit direkter Plasmaeinwirkung ermöglicht.

Der entwickelte Aufbau vermeidet Einflüsse durch Gefäßwände und erlaubt eine unabhängige Steuerung der Temperatur. Dies wird durch den kombinierten Einsatz eines CO_2-Lasers zur Aufheizung und eines kalten Atmosphärendruckplasmas zur Anregung chemischer Reaktionen erreicht. Ergänzend wurde ein Diagnostiksystem integriert, das die Beobachtung und Bewertung der Proben während des Prozesses ermöglicht. Konstruktive Maßnahmen zur elektrischen Isolation und thermischen Stabilisierung gewährleisten einen zuverlässigen Betrieb.

Die Ergebnisse zeigen, dass die Kopplung von aerodynamischer Levitation und DBD-Plasmajet technisch umsetzbar ist. Es konnte eine stabile Levitation mit gleichzeitigem Plasmaeintrag demonstriert werden, womit ein neues Experimentierfeld für die Untersuchung von Oxidations- und Reduktionsprozessen eröffnet wurde. Damit schafft der Reaktor die Grundlage für eine präzisere Charakterisierung von Materialien unter praxisnahen Bedingungen und eröffnet Perspektiven für weiterführende Studien zur Kinetik von Oberflächenreaktionen und zur zeitaufgelösten Diagnostik.

Acknowledgements

At this point I would like to express my heartfelt gratitude to all those who supported me during my Master's studies and in particular throughout the course of this thesis.

My deepest thanks go to my family. The foundation for my educational path was laid by my grandparents, whose courage to emigrate created the opportunity for me to pursue this journey in the first place. I am sincerely grateful to my parents and my sister, who have always stood by me with unwavering support, whether through advice, encouragement or financial help. Without their care, trust and belief in me, this thesis would not have been possible. I would also like to thank my uncles and aunts, who have always been a reliable source of strength.

My gratitude also goes to all those who made this work academically possible. Professor Rudolf Neu provided the academic framework by supervising my thesis and giving me the opportunity to realize it in its full scope. I would also like to thank my supervisors at DLR, Dr. Hubertus Thomas and Dr. Mikhail Pustylnik, who supported me throughout the entire process, guided me with their expertise, and were always available whenever I faced questions or difficulties.

I am especially grateful to my friends, who have been a source of strength and joy over the years. Enes Kesimal has accompanied me since my Bachelor studies, and together we have overcome every hurdle of our academic journey. I am deeply thankful for this long-standing friendship, built on mutual trust and countless shared memories. I also wish to thank Selin Altun, who was an important emotional support during my time in Munich and helped me stay on course with her encouragement and presence. A special thanks also goes to Jacquelin Volz and Magnus Behrendt, who always listened to my concerns and helped me overcome challenges.

I would further like to thank the people I met during my Master's studies who made this time such a special chapter of my life. Abdurrahman Demirci and Furkan Demir hold a truly special place in this regard. In the final phase of this thesis, they were not only a source of practical advice and help but also an unwavering emotional support. Their friendship, motivation and belief in me gave me the strength to persevere through difficult moments and ultimately complete this work. Alongside them, I am also deeply grateful to my Erasmus friends Riccardo, Andrea, Martina, Sonia, Antonio and Laura. With them I was able to form friendships that transcend national borders, and they inspired me with their cultures, perspectives and expertise in their respective fields. Both through their personal support and the academic exchange we shared, they enriched my journey in a unique way, showing me, how valuable diversity can be for personal growth and for approaching research with new ideas and renewed motivation

Above all, I wish to thank a person who has been truly special to me, Zeyna Maria Yabanci. Among everyone, she gave me the greatest support in completing this thesis. She stayed by my side through long days and nights, shared her energy and emotions with me, and never let me face this challenge alone. Her presence, dedication and support have been invaluable, and for that I am deeply and sincerely grateful.

Table of Contents

List of Figures

List of Tables

Table of Acronyms

Acronym	Description
ADL	Aerodynamic Levitation
AL	Acoustic Levitation
APPJ	Atmospheric Pressure Plasma Jet
CO_2	Carbon Dioxide
DBD	Dielectric Barrier Discharge
DLR	German Aerospace Center
EML	Electromagnetic Levitation
ESL	Electrostatic Levitation
FWHM	Full Width at Half Maximum
HV	High Voltage
ICCD	Intensified Charge-Coupled Device
LTP	Low-temperature plasmas
PA	Polyamid
PLA	Polylactic Acid
RF	Radio Frequency
ZnSe	Zinc Selenide
NaCl	Sodium Chloride

Symbols and Indices

Latin Symbols

Symbol	Meaning	Unit
A	Projected area	m^2
F_g	Gravitational force	N
F_l	Aerodynamic lift force	N
f	Frequency	Hz
g	Gravitational acceleration	$\frac{m}{s^2}$
$J(r)$	Current density at a depth r	$\frac{A}{m^2}$
J_0	Surface current density	$\frac{A}{m^2}$
m	Mass	kg
p_d	Dynamic pressure of the gas jet	Pa
r	Radius	m
v	Gas flow velocity	$\frac{m}{s}$

Greek Symbols

Symbol	Meaning	Unit
ρ	Density	$\frac{kg}{m^3}$

1 Introduction

“There may possibly be an entirely new world, a world of matter between gases and radiant matter.” – William Crookes, 1879

With these words, Crookes described for the first time what we now know as plasma, the fourth state of matter. Plasmas not only shape natural phenomena such as lightning and auroras but have also become versatile tools in science and technology [1, 2].

Materials research represents a central field of application where plasmas open up new experimental opportunities. How this potential is addressed within the present work is outlined in the following motivation. Building on this, the objectives are specified and the main steps are described that are taken to achieve them.

1.1 Motivation

Low-temperature plasmas (LTP), characterized by a strong non-equilibrium between highly energetic electrons and comparatively cool heavy particles, have emerged over the past decades as a versatile field of research and application. In contrast to thermal plasmas, where electron and gas temperatures are nearly balanced, cold plasmas enable the generation of highly reactive species such as radicals, ions, and metastable states at moderate bulk temperatures. This allows chemical processes to be initiated selectively without imposing excessive thermal loads on the system. [3]

These unique properties have led to significant advances across many areas of science and technology. In microelectronics, they are indispensable for the deposition, structuring, and modification of thin films. Processes such as plasma-enhanced chemical vapor deposition or plasma etching would not be feasible without this technology. In medical technology, cold plasmas are used for sterilization, microbial inactivation, and increasingly in plasma medicine for targeted tissue treatment and wound healing. In environmental technology, they enable the removal of pollutants from air and water, the reduction of nitrogen oxides, and the decomposition of complex molecules, thus offering a sustainable alternative to conventional cleaning methods. Moreover, energy research has shown growing interest in plasma-assisted processes such as CO_2 reduction, efficient hydrogen production, and nitrogen fixation, all of which are highly relevant in the context of climate change and the energy transition. [3]

An expanding field of research is materials science, where low-temperature plasmas provide new experimental opportunities. They can be employed to functionalize surfaces, modify wetting behavior, or initiate interfacial reactions. Particularly relevant is their potential to trigger redox processes in high-temperature materials without subjecting the entire system to thermal stress [1],. [3]

However, fully exploiting this potential is challenging with existing methods. The investigation of high-melting oxides and reactive materials remains severely limited, as crucibles or holders inevitably lead to chemical interactions and measurement artifacts. While aerodynamic levitation (ADL) provides an established solution for containerless experiments [4], it has so far been applied mainly in combination with thermal plasmas. Their major drawback lies in the

inseparable coupling of temperature and plasma-chemical effects. Oxide reduction requires sufficient thermal activation, yet the reactive species generated in the plasma are equally decisive for the reaction. In thermal plasmas, these contributions cannot be independently controlled, preventing a systematic analysis of the underlying mechanisms and increasing the risk of overheating or undesired melting of the sample. [5]

Cold atmospheric pressure plasmas, particularly dielectric barrier discharge Jets (DBD-Jets), offer a decisive advantage by enabling targeted activation of chemical processes at moderate temperatures [3]. Nevertheless, an integrated system that combines ADL and plasma functionality in a single setup has not yet been realized. This research gap defines the starting point of the present work.

Its central innovation lies in the development of a reactor that, for the first time, integrates ADL and DBD-Jet plasma into a single design. The distinguishing feature of this approach is the ability to control the sample temperature via a laser independently of the plasma conditions. As a result, thermal and plasma-related effects can be systematically decoupled. This separation opens up new research opportunities, allowing oxidation and reduction processes to be investigated under realistic conditions with controlled variation of temperature and plasma parameters.

The combined reactor thus addresses a critical research gap and establishes a platform of high relevance both for fundamental studies and for application-oriented developments in materials processing

1.2 Objective of the Work

The overarching aim of this thesis is the development and demonstration of a reactor that combines the aerodynamic levitation of millimeter-sized samples with a dielectric barrier discharge plasma jet (DBD jet). This system is designed to enable crucible-free investigation of materials while simultaneously subjecting them to targeted plasma exposure.

A central distinguishing feature of the reactor lies in its ability to adjust the sample temperature independently of the plasma conditions by means of laser heating. This allows thermal and plasma-related effects to be systematically decoupled and their respective contributions to material behavior to be analyzed with precision.

To achieve this aim, three key objectives are pursued:

- the experimental determination of plasma ignition conditions,
- the conceptual design and CAD-based construction of the reactor,
- the fabrication and integration of the reactor into the existing levitation facility at the DLR Institute Frontier Materials on Earth and in Space (see Chapter 4).

The aim of this thesis is considered accomplished once the developed reactor enables both stable levitation and reliable treatment of samples with cold plasma within an integrated experimental setup.

1.3 Thesis Structure

This thesis is divided into six chapters. Following the introduction, Chapter 2 presents the state of the art. It reviews levitation techniques and plasma processes with a particular focus on their applications in materials science. From this analysis, the research gap is identified that is addressed by the reactor developed in this work.

Chapter 3 provides the theoretical background. It covers the physical principles of levitation, the generation and guidance of cold dielectric barrier discharge (DBD) plasma jets at atmospheric pressure, the influence of electrode geometry, and the interaction between plasma and the sample surface.

Chapter 4 describes the methodology. The existing ADL system, including the levitation unit, heating, diagnostics, and process chamber, is characterized, and the plasma behavior is experimentally analyzed. Parameters such as ignition conditions, electrode spacing, polarity, and nozzle geometry are investigated. In addition, the coupled plasma–levitation system is examined.

Chapter 5 presents the results and discussion. It includes the final reactor design and the demonstration of stable levitation under plasma operation. Chapter 6 concludes the thesis with a summary of the main findings, evaluates the achieved functional scope of the reactor, and discusses limitations and optimization potential of the developed setup.

2 State of the Art

Levitation techniques have become an established method in material science to process samples without a container, thereby avoiding contamination or interference from crucibles or holders [4]. This enables the precise determination of intrinsic material properties, as external influences are excluded [4]. Among the established methods are acoustic, electrostatic, electromagnetic and aerodynamic levitation [4, 6–8].

Aerodynamic levitation (ADL) is particularly advantageous, as it allows stable confinement of samples heated to very high temperatures [4]. Owing to this ability to process melts at several thousand degrees Celsius without container interaction, Benmore and Weber [9] employed ADL to generate strongly undercooled liquids and thereby synthesize metastable crystalline and glassy phases. The non-contact environment of ADL further permits precise thermophysical property measurements, which Gong et al. [10] used to determine viscosity, density and surface tension of corium components.

To reach and control such high temperatures, aerodynamic levitation experiments typically employ CO_2 laser heating, as oxide materials strongly absorb at the laser wavelength of 10.6 µm [11]. In many setups, a single laser is directed onto the levitated droplet, which enables rapid heating but often results in pronounced vertical temperature gradients and asymmetric sample shapes [11]. These gradients can compromise measurements of volume and density, as well as affect the stability of the levitation [11, 12]. To mitigate this, two-laser configurations are increasingly used, in which the sample is irradiated from both above and below. This arrangement significantly reduces internal temperature gradients and ensures a more homogeneous thermal field across the droplet [11, 12]. The use of dual lasers has thus become the standard in precision studies, as it stabilizes the sample position and improves the reliability of thermophysical data. In terms of technical requirements, CO_2 lasers with powers on the order of 100–400 W are commonly applied, since this range is sufficient to melt refractory oxides and maintain stable liquid states under levitation [4, 11]. Furthermore, the combination of controlled laser heating and a reducing gas atmosphere enables redox reactions, allowing, for example, the targeted reduction of metal oxides and the study of oxygen exchange processes in high-temperature melts. [4]

In parallel, plasmas have gained considerable importance in materials processing. They enable not only thermal influence but also chemical modification of materials through reactive species [13–15] Non-thermal atmospheric pressure plasmas are of special relevance since they generate radicals, ions, and metastables through electron impact processes while keeping the bulk gas temperature comparatively low [16–18]. This property makes it possible to initiate redox reactions under conditions that would otherwise require extreme thermal input.

This capability has attracted increasing attention in the context of oxide reduction, particularly regarding carbon-free ironmaking. Conventional iron ore reduction is based on coke as a reductant, which leads to high CO_2 emissions [19]. Hydrogen has been identified as a sustainable alternative since its only reaction product is water [20]. However, purely thermal reduction with H_2 is strongly endothermic and requires temperatures above ~750 °C to achieve sufficient reaction rates, which in practice leads to complications such as sintering of the ore. Non-thermal plasmas address this limitation by activating hydrogen through electron impact

dissociation and vibrational excitation, thereby enabling efficient reduction kinetics at substantially lower substrate temperatures. [16–18]

Experimental evidence supports this concept. Udachin et al. [16] showed that iron oxide films exposed to a dielectric barrier discharge in Ar/H_2 at atmospheric pressure were almost completely reduced within 10 s at only 200–300 °C, whereas purely thermal hydrogen treatment under the same conditions produced negligible effects. The acceleration was attributed to plasma-generated atomic hydrogen and vibrationally excited H_2 molecules. [16] Similarly, Kumar et al. [17] demonstrated that non-thermal microwave plasmas at atmospheric pressure could reduce iron ore powders with rates three to four times faster than conventional thermal processes. Although the bulk gas in their system still reached elevated temperatures, the decisive contribution was the reactivity of plasma-activated hydrogen species. [17]

Ellis et al. [18] provided particularly valuable insights by decoupling surface heating from plasma exposure. Using a microwave-driven non-thermal plasma jet, they treated iron oxide samples while independently controlling the substrate temperature between 280 °C and 500 °C. Their results confirmed that, at these moderate temperatures, thermal hydrogen alone was insufficient to drive reduction, whereas plasma-generated hydrogen radicals enabled rapid conversion with an apparent activation energy of only ~50 kJ/mol. Importantly, they emphasized that both temperature and plasma conditions must be considered as independent parameters. The most efficient reductions were achieved when moderate thermal input and high radical densities acted in combination. At the same time, the study highlighted that a systematic investigation of plasma-driven redox reactions requires an experimental setup that allows the independent variation of thermal and plasma contributions. [18]

The idea of combining levitation techniques with plasma processes is compelling, as it allows samples to be heated in a containerless state while simultaneously being exposed to a chemically active environment. In the literature, only a few approaches have been reported that explore such combinations, each with different objectives and limitations.

Snabre et al. [8] investigated aerodynamic levitation in combination with a thermal plasma. They levitated metallic spheres of 6–8 mm diameter in a turbulent argon plasma jet generated by a DC arc. The plasma stream simultaneously provided the levitating gas flow and served as a high-temperature heat source. This setup enabled stable levitation and heating of the rotating spheres without contact. The study focused on convective heat transfer at the particle surface and demonstrated that free particle rotation significantly alters the heat transfer compared to fixed geometries. Although the work successfully combined aerodynamic levitation and plasma, the plasma was purely thermal and no chemical reactions were investigated. [8]

A related concept was described in a patent by Leung and Man [15], who proposed to couple various levitation methods, including aerodynamic, electromagnetic, electrostatic, or acoustic levitation, with plasma torches for heating. The plasma torch at atmospheric pressure was intended to melt levitated samples under containerless conditions, while magnetic coils or electrodes stabilized the plasma environment around the sample. The purpose was mainly directed towards containerless melting for microgravity research. However, this approach remained at the conceptual level, as no experimental realization was published. [15]

Other combinations involved acoustic levitation with plasmas used as diagnostic tools. Contreras et al. [6] levitated microliter water droplets using acoustic fields and applied laser-

induced breakdown spectroscopy (LIBS). A pulsed laser generated a transient plasma within the droplet, enabling trace analysis of heavy metals such as Ba, Cd, Hg, and Pb at ppm concentrations. In this case, the plasma served exclusively as an analytical probe, while no sustained chemical modification of the levitated sample was performed. [6]

Electrostatic levitation in plasma environments has also been explored for material synthesis. Shimizu et al. [13] levitated micrometer-sized diamond seeds in a radio-frequency (RF) plasma using CH_4/H_2 mixtures and demonstrated homoepitaxial diamond deposition on the levitated particles. [13] Similarly, Praburam and Goree [14] studied nanoparticle formation inside an RF discharge, where particles remained suspended due to electrostatic charging. These studies highlight how plasmas can act simultaneously as levitating media and chemically reactive environments, but they did not involve aerodynamic levitation and did not target redox chemistry. [14]

A closer step towards redox processes was reported by Pack et al. [4], who combined aerodynamic levitation with reactive gas atmospheres. Oxide and silicate samples of 2–3 mm diameter were levitated in an argon stream and heated above 2000 °C using a CO_2 laser. By adding hydrogen, the authors demonstrated thermal reduction of Fe-, Ni-, and Co-bearing oxides, leading to metallic exsolution. Although these experiments successfully coupled aerodynamic levitation with reduction reactions, the driving force was purely thermal, as no cold plasma source was applied. [4]

A further intriguing observation was made by Poulain et al. [7], who demonstrated that plasma itself can induce levitation. In their study, aqueous droplets placed on a heated metal plate could levitate once a sufficiently high voltage was applied. The phenomenon was attributed to the formation of a plasma-supported gas cushion beneath the droplet, reminiscent of a Leidenfrost-like effect. While this work highlighted an unusual mode of plasma-assisted levitation. [7]

The review of existing studies reveals a clear research gap. While various attempts have been made to combine levitation techniques with thermal plasmas or diagnostic plasma sources, no study has yet reported the coupling of aerodynamic levitation with a cold dielectric barrier discharge (DBD) plasma jet for the targeted investigation of oxidation–reduction reactions. Pack et al. [4] demonstrated that oxide reduction can be achieved in levitated melts, but the process was purely thermally driven and did not involve a cold plasma environment.

At the same time, extensive research on non-thermal atmospheric pressure plasmas has shown that reactive species such as atomic hydrogen or oxygen can drastically accelerate redox reactions [16–18]. In particular, Ellis et al. [18] emphasized the importance of decoupling thermal and plasma effects in order to identify the specific contribution of plasma-generated radicals.

Thus, a decisive gap remains: The advantages of aerodynamic levitation, contact-free stabilization at high temperatures and the elimination of container interactions, have not yet been combined with the potential of cold atmospheric plasmas that can trigger redox reactions even at temperatures close to room temperature. The present work addresses this gap by developing a novel reactor concept in which the sample temperature and plasma parameters can be adjusted independently. This approach provides, for the first time, an experimental platform for the systematic investigation of oxidation and reduction processes under containerless conditions with cold plasma exposure.

3 Theory

As outlined in the previous chapter, the combination of aerodynamic levitation with a dielectric barrier discharge jet opens up new possibilities for investigating chemical processes, in particular oxidation and reduction reactions. However, the construction of such a reactor requires a thorough understanding of the underlying physical and chemical mechanisms. This chapter therefore covers the theoretical principles necessary for the design and layout of the reactor.

3.1 Fundamentals of Levitation

Levitation refers to the contactless floating of an object in a stable position without mechanical support or container. The term is derived from the Latin levitas, meaning “lightness” [21]. Physically, levitation is achieved when an upward force compensates for the gravitational force acting on a sample. In addition to the pure balance of forces, stability is particularly crucial: If the sample is deflected from its equilibrium position, a restoring force should return to the equilibrium point. In this way. The sample is kept afloat without any containment, which is of great advantage in materials research, as interactions with crucibles can be avoided and intrinsic material properties can be precisely investigated [22].

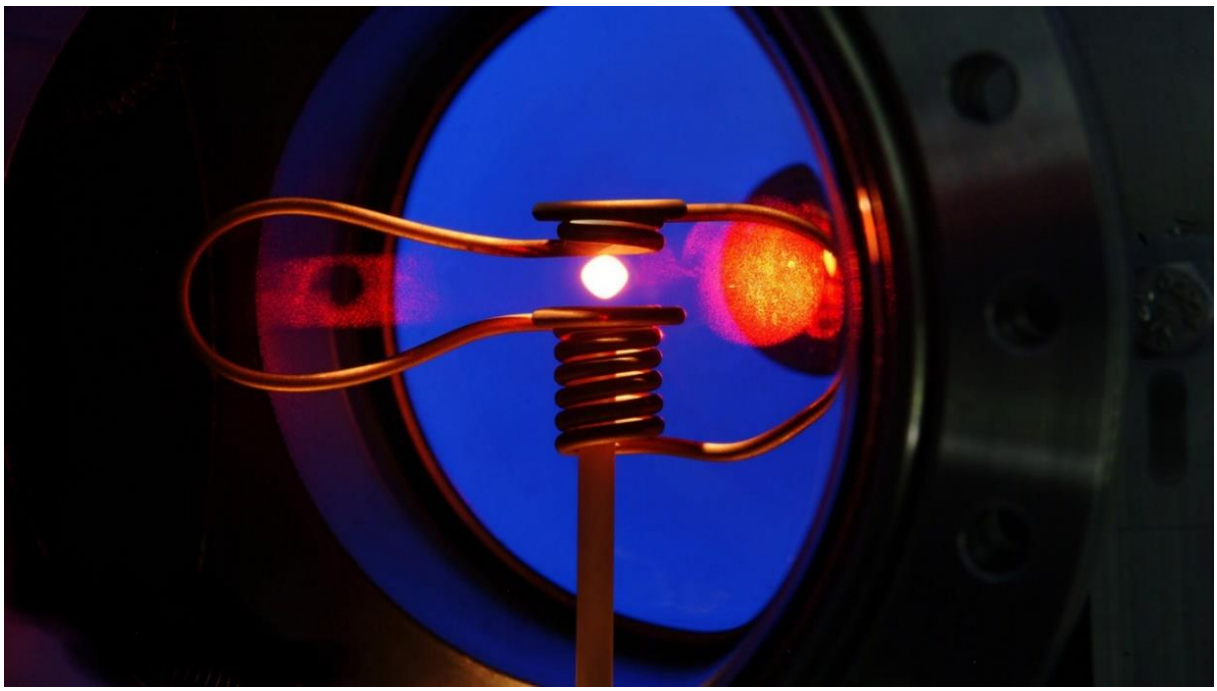

Figure 3.1: A molten metal sample was levitated by electromagnetic forces and maintained in a free-floating state for 20 seconds of weightlessness achieved during a parabolic flight. [23]

There are basically four different methods of levitation, each based on different physical principles [4]. In electromagnetic levitation (Figure 3.1), an electrically conductive sample is placed in a high-frequency magnetic field, which induces eddy currents. According to Lenz's law, these generate an opposite magnetic field, which causes a Lorentz force and stabilizes the sample [24]. Electrostatic levitation (ESL), on the other hand, is based on Coulomb forces acting on an electrically charged sample. To achieve this, the object is positioned between

oppositely charged electrodes, requiring active control to keep the sample in stable suspension [25].

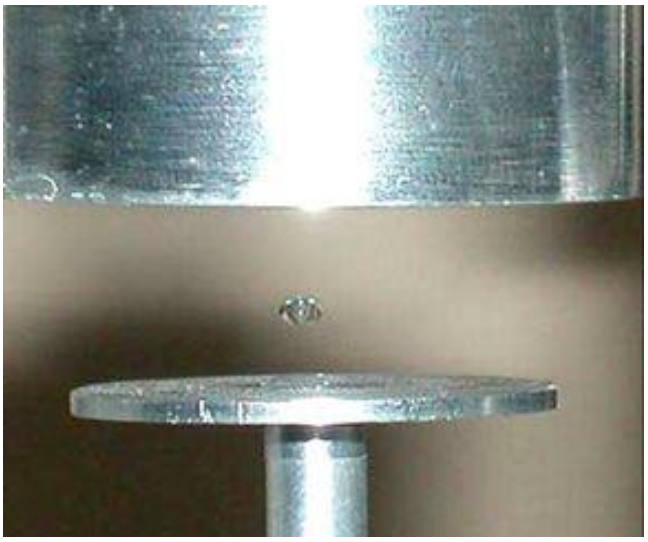

Figure 3.2: An experimental setup demonstrates acoustic levitation, in which a droplet is maintained in stable suspension at the node of a standing ultrasonic wave formed between a piezoelectric transducer located at the bottom and a reflector positioned at the top. [26]

Acoustic levitation (Figure 3.2) uses high-intensity ultrasonic waves that generate a standing wave field. Pressure minima are created at the nodes of this standing wave, in which small objects can be fixed and stabilized [27]. Finally, aerodynamic levitation (Figure 3.3) employs a drag force which the gas flow exerts on a sample, usually a spherical melt. Stabilization effects ensure that lateral deflections are compensated and the sample is fixed in the flow axis [7, 8].

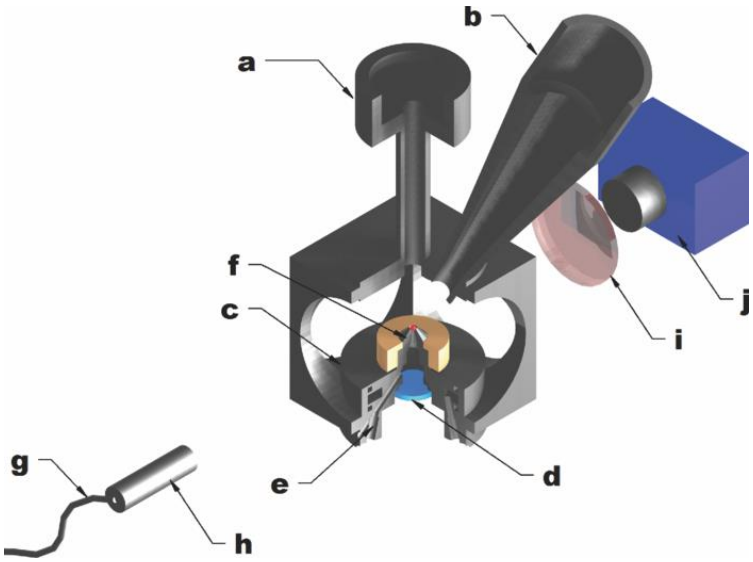

Figure 3.3: Levitation process chamber based on a ThorLabs 60 mm optical cube. Main components: (a) top laser port, (b) pyrometer head tilted ~30° from vertical, (c) water-cooled levitation stage, (d) ZnSe/NaCl window transparent at 10.59 µm, (e) levitation gas inlet, (f) aerodynamic converging–diverging nozzle with 1.2 mm central opening, (g) back-lighting laser source (200 mW, 660 nm), (h) beam-expanding optics producing an ~11 mm beam, (i) 660 nm bandpass filter (10 nm FWHM), and (j) high-speed camera (800 fps) with a telecentric lens. [28]

Each of these methods has specific advantages and disadvantages. For the objective of this work, two criteria are particularly decisive: compatibility with a dielectric barrier discharge (DBD plasma) and the feasibility of carrying out oxidation and reduction reactions under defined conditions. In the context of plasma coupling, two additional requirements arise. First, the levitation method must not rely on external electromagnetic fields, as these would interfere with the discharge process. Second, stable levitation must be possible at pressures close to atmospheric conditions, since the plasma jet operates in this regime. Table 3.1 summarizes the strengths and weaknesses of the four methods with respect to these criteria. It becomes evident that both aerodynamic levitation and acoustic levitation fulfill these requirements, as they operate at atmospheric pressure and do not require high-frequency fields for stabilization. However, within the framework of this work, aerodynamic levitation was defined as the levitation technique, since a functional levitator was already in operation at the institute and served as the basis for further developments. Therefore, all subsequent investigations are conducted using this method.

Table 3.1: Comparison of EML, ESL, AL, and ADL regarding coupling with plasma. [7, 8, 24, 25, 27]

Method	Physical principle	Sample type & environment	Suitable for plasma
Electromagnetic levitation	Lorentz force on induced eddy currents in conductive samples; inductive levitation and melting	Electrically conducting samples; mostly inert atmospheric or vacuum to avoid arcing and oxidation	No, HF field interference with plasma
Electrostatic levitation	Static Coulomb forces on charged samples in high cacuum; stabilization via active control	Conductive and non-conductive samples (mm-size); requires high vacuum; laser heating possible	No, vacuum is needed
Acoustic levitation	Acoustic radiation force in ultrasonic standing wave; levitaion at pressure nodes	Small samples, (<< wavelength, typically < 5mm); air or controlled atmosphere; heating possible	Yes
Aerodynamic levitation	Flow lift genrated by gas jet; stabilization by Bernoulli effect	Mainly spherical samples (1-5mm); typical carrier gas Ar or He (with additives); atmospheric or elevated pressure; laser heating possible	Yes

3.1.1 Physical Principles and the relevant Stabilizing Effects

Aerodynamic levitation is based on the balance between the weight of the sample and the aerodynamic lift generated by the gas jet (Figure 3.4). For a spherical sample with radius r and density ρ, the weight is given by

$$F_g = mg = \frac{4}{3}\pi r^3 \rho_p g \qquad (3.1)$$

where g denotes the acceleration due to gravity.

The lift force generated by the nozzle can be determined via the dynamic pressure p_d on the projected area of the sphere A:

$$p_d = 1/2\rho_g v^2 \; with \; A = \pi r^2 \qquad (3.2)$$

where ρ_g is the gas density and v is the flow velocity. This results with the drag coefficient c_d in the following to the aerodynamic lift force:

$$F_l \approx c_d \frac{1}{2}\rho_g v^2 \pi r^2 \qquad (3.3)$$

A stable levitation state is achieved when the lifting force balances the gravitational force $F_l \approx F_g$. This balance of forces has been experimentally confirmed for various ADL systems. [29]

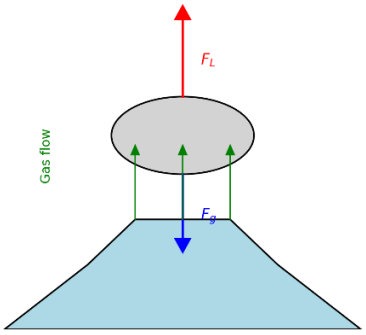

Figure 3.4: Schematic representation of the force balance in aerodynamic levitation.

An important stabilization effect of a levitated sample in an aerodynamic gas stream can be explained by the Bernoulli principle (Figure 3.5). As the velocity of the surrounding gas increases, the static pressure decreases, which generates a horizontal restoring force that centers the sample along the axis of the flow. In addition to the vertical lift produced by the drag force of the gas jet, pressure differences on opposite sides of the sample create a restoring momentum that continuously drives the particle back toward its equilibrium position. This effect ensures that the levitated sample remains aligned with the jet axis, even when it is slightly displaced from the center. [30]

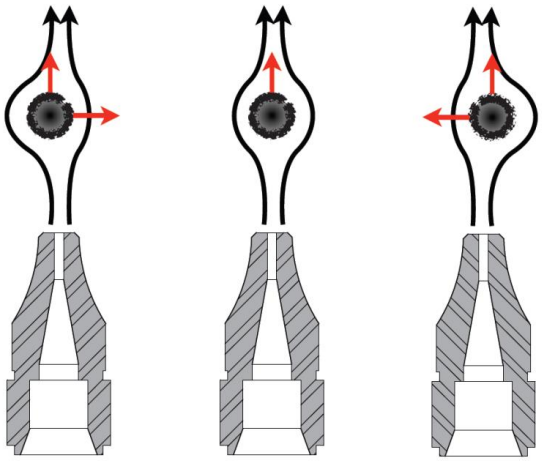

Figure 3.5: Application of Bernoulli's principle to levitation. The flow-induced suction counterbalances the gravitational force on the spherical sample, and the resulting pressure distribution confines it to the central axis. [30]

3.2 Atmospheric Pressure Plasma Technologies

Plasma is an ionized gas and is often referred to as the fourth state of matter alongside solid, liquid, and gas. [31] It contains free electrons, ions, and neutral particles and therefore exhibits electrical conductivity. Plasmas can occur both as thermal equilibrium plasmas with high gas and electron temperatures and as non-equilibrium plasmas. In the latter case, the electron temperature is in the range of electron volts, while the gas temperature remains close to ambient temperature. [32] Atmospheric pressure plasmas are particularly interesting for

technological applications since they do not require expensive vacuum equipment and provide a high density of reactive species while placing only a low thermal load on substrates. [33]. Atmospheric pressure plasmas can be operated directly in air or process gases and can therefore be easily integrated into production lines. [34]

3.2.1 Dielectric Barrier Discharges and Streamer Physics

A widely used method to generate non-equilibrium plasmas at atmospheric pressure is the dielectric barrier discharge (DBD). In this configuration, at least one of the electrodes is covered by a dielectric material such as quartz, alumina, or ceramic. When an alternating high voltage is applied, typically in the kilovolt range at frequencies from a few kilohertz to several tens of megahertz, the gas between the electrodes breaks down once the applied electric field exceeds the local ionization threshold. The dielectric layer limits the discharge current by accumulating surface charge, which counteracts the external field and rapidly quenches the current pulse. This mechanism prevents the transition into a thermal arc and instead produces a multitude of short-lived microdischarges that together form a cold plasma at atmospheric pressure. [35]

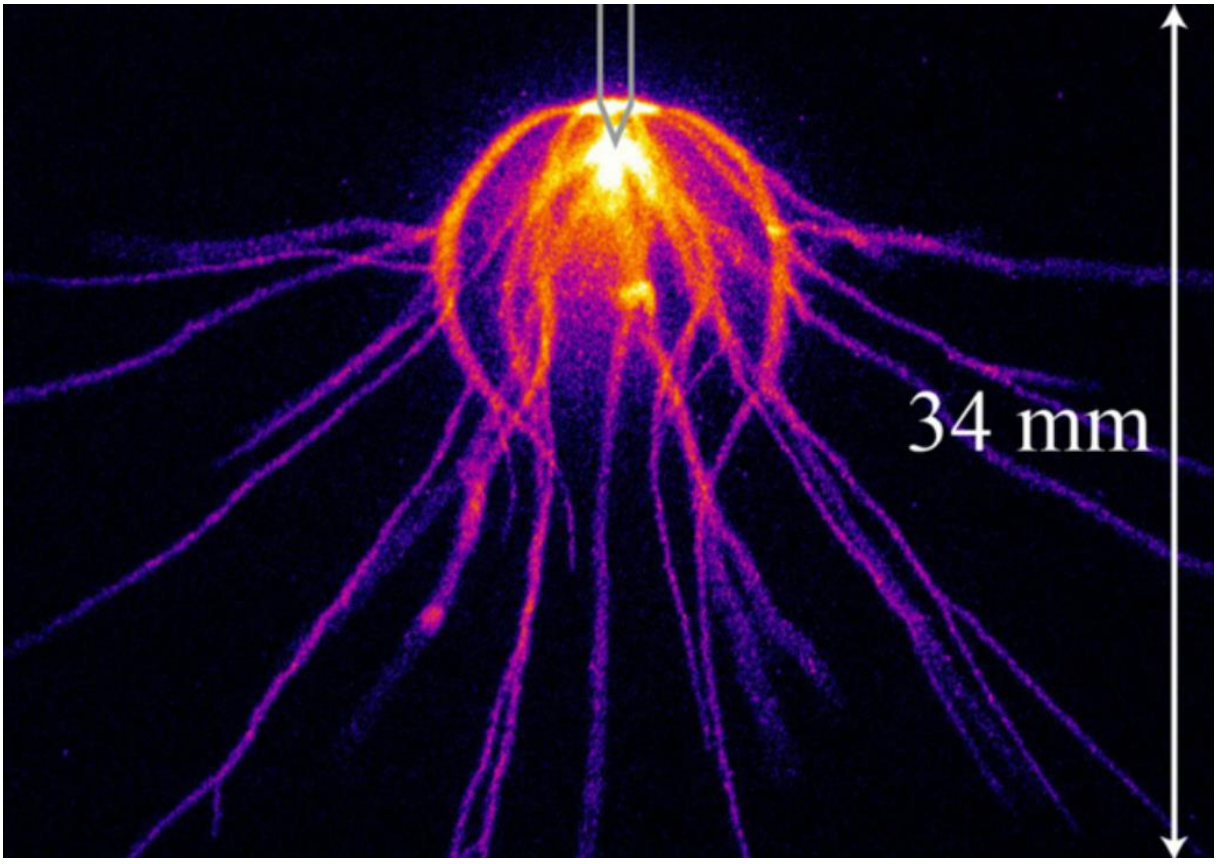

Figure 3.6: A 3 µs exposure false-color image capturing an unusual streamer discharge produced under the influence of a complex voltage pulse. [36]

The fundamental building blocks of DBD microdischarges are streamers (Figure 3.6). A streamer is a thin, filamentary ionization channel that propagates rapidly through the neutral gas, sustained by the strong enhancement of the electric field at its head. Streamers typically originate from initial electron avalanches that, after reaching a critical size, generate space charge layers. These space charges distort and enhance the local electric field at the

avalanche front, thereby enabling self-sustained propagation of the ionization front [36]. The head of a positive streamer is characterized by a compact cloud of electrons at the tip and a trail of positive ions left behind, producing a localized field enhancement that accelerates electrons up to several electronvolts. These electrons cause further ionization and excitation, ensuring continuous advancement of the discharge front. [36, 37]

An essential mechanism that enables the propagation of positive streamers, especially in molecular gases such as air, is photoionization. Ultraviolet photons emitted by excited nitrogen and oxygen species in the streamer head ionize neutral molecules in the volume ahead of the front. This process generates seed electrons in regions that are not directly connected to the electrode, which are then accelerated by the local electric field into secondary avalanches [5]. In this way, photoionization provides the necessary electron density ahead of the streamer to sustain its rapid propagation at velocities in the order of 10^5 m/s, much faster than electron drift in the undisturbed background field [36, 38].

At atmospheric pressure, the transition from Townsend avalanches to streamers occurs almost inevitably once the electric field exceeds the breakdown threshold in gaps larger than a few hundred micrometers [37]. Consequently, DBDs at atmospheric pressure do not form homogeneous Townsend discharges but instead consist of numerous filamentary streamers that ignite and extinguish within nanoseconds. The dielectric ensures that these filaments terminate on the surface, where their charge deposition locally suppresses further breakdown until the field reverses with the next half-cycle of the applied voltage. Macroscopically, this sequence results in a quasi-homogeneous cold plasma, while microscopically it is governed by the repetitive dynamics of streamer initiation and extinction. [36, 37]

3.2.2 DBD Plasma Jets

A specific configuration of dielectric barrier discharges is the DBD plasma jet, in which the generated plasma is expelled as a free jet into the surrounding atmosphere. Typically, a plasma jet consists of a dielectric capillary tube (e.g., quartz or ceramic) through which a feed gas such as helium or argon flows (see Figure 3.7). Electrodes are arranged in such a way that a discharge ignites inside the capillary, and the ionized gas is transported outward by the gas flow. At the nozzle exit, this results in a luminous plasma plume that extends several millimeters to centimeters into the ambient air. [33, 39]

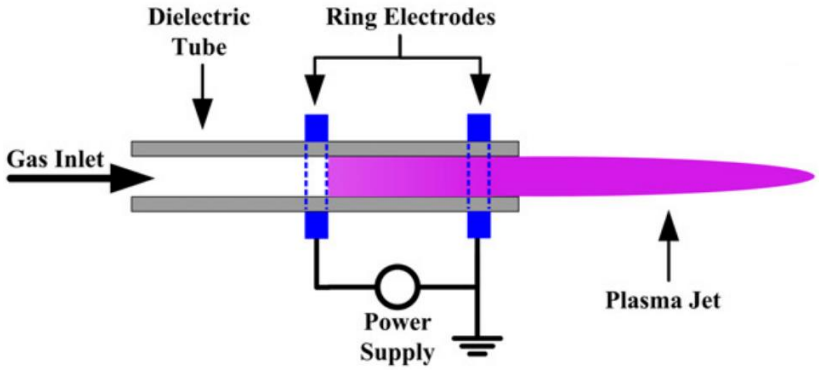

Figure 3.7: Schematic structure of a DBD plasma jet. The quartz tube acts as a dielectric, the ring-shaped electrodes couple the field into the gas and the visible plasma jet forms at the outlet. [40]

A characteristic feature of many DBD plasma jets is the formation of discrete, temporally separated plasma fronts known as plasma bullets. High-speed imaging has revealed that these ionization wave packets propagate with velocities of 10^4 to 10^5 m/s, which is orders of magnitude faster than the actual gas flow [39]. Unlike a continuously blown flame, these jets are in fact streamer-like ionization waves driven by the applied electric field. This phenomenon was first reported by Teschke et al. through time-resolved ICCD photography [39].

The formation of a plasma bullet can be described as follows: during one half-cycle of the applied voltage, a primary discharge streamer ignites inside the capillary and ionizes the feed gas. After the discharge current decays, a locally charged and metastably excited gas volume remains, which detaches from the electrode region and propagates as a self-sustaining plasma front into the surrounding atmosphere. These ionization shock fronts appear as bright, projectile-like light structures that are regenerated with each voltage half-cycle. Their extension and intensity strongly depend on parameters such as feed gas type, flow rate, driving frequency, and electrode configuration. [39, 41]

An essential characteristic of plasma jets is their ability to transport chemically active species such as radicals and metastables beyond the nozzle, while the overall gas remains close to room temperature. This makes them particularly suitable for the treatment of sensitive materials or biological tissues [33, 39, 41]. In materials science, the capacity to deliver reactive plasmas in a spatially localized and controlled manner is exploited for surface modification, thin film processing, or reduction reactions.

3.2.2.1 Influence of Electrode Polarity and Geometric Aspects

The properties of a DBD plasma jet are highly sensitive to the electrode configuration and the applied polarity. The spatial distribution of the electric field, as well as the point of streamer initiation, is largely determined by whether the nozzle electrode is connected to high voltage or ground (see Figure 3.8). In symmetrical AC excitation, the polarity alternates every half-cycle, which leads to alternating discharge dynamics.

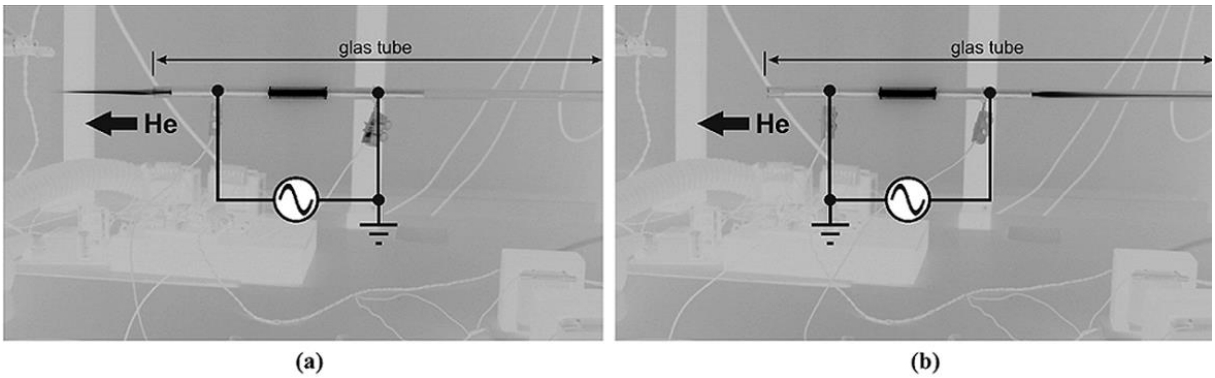

Figure 3.8: Inverted photographs illustrating the influence of electrical connections on the plasma jet position: (a) downstream configuration and (b) upstream configuration. [39]

Experiments (see Figure 3.9) have shown that when the nozzle electrode acts as the cathode, intense and well-focused plasma bullets are launched from the nozzle orifice into the ambient atmosphere. In contrast, when the nozzle is biased as the anode, the resulting plasma bullets are broader and less luminous [41]. This difference is attributed to the fact that in the cathode-driven case, dense electron avalanches form directly at the nozzle edge, producing strong positive streamers that propagate outward with high velocity. In the anode-driven case, the

initial avalanches start at the inner cathode electrode, and by the time they reach the nozzle exit, their space charge has already partly dissipated, resulting in weaker, more diffuse bullets [33, 41].

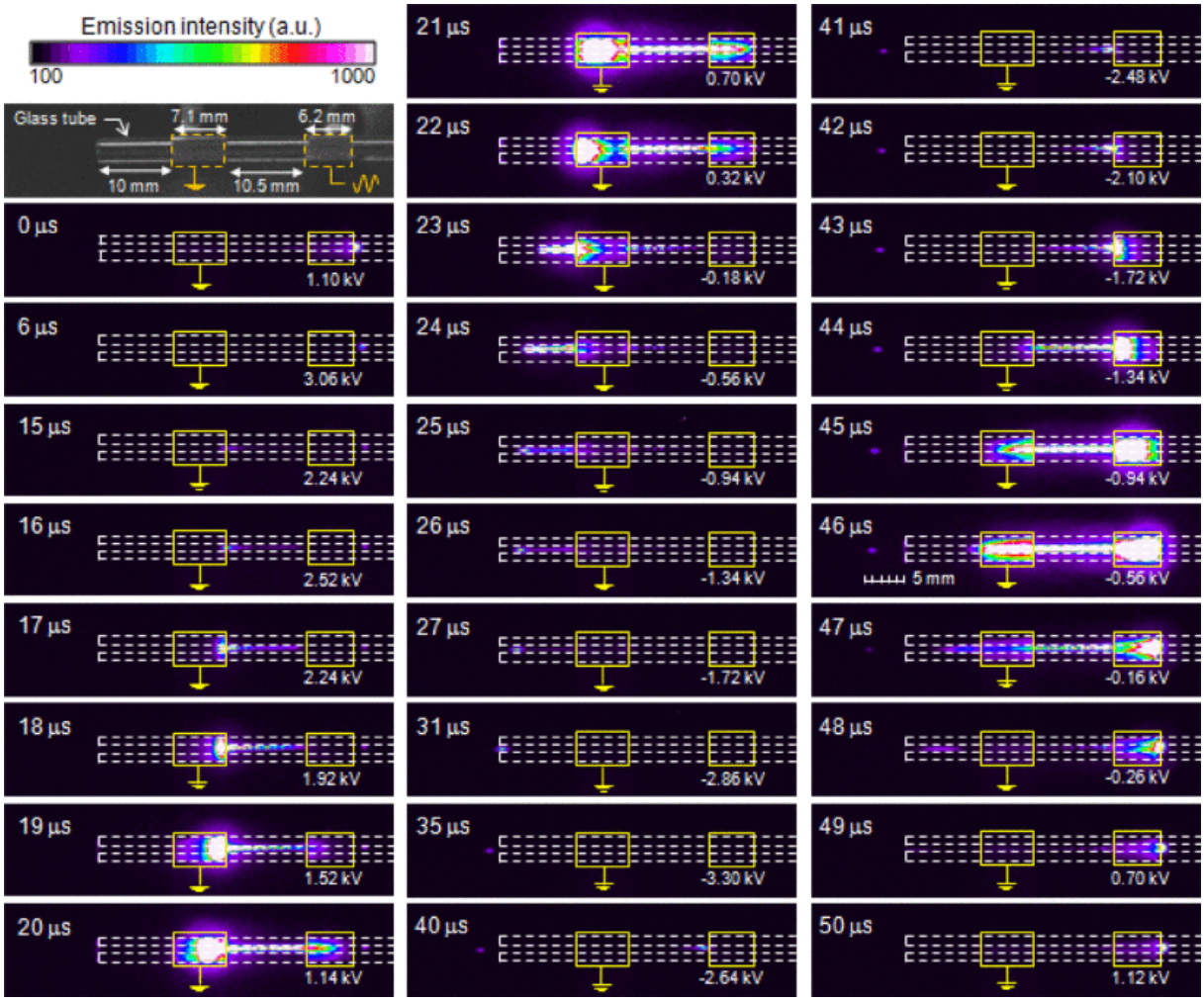

Figure 3.9: CCD camera images with 1 µs exposure capture the time evolution of a capillary DBD atmospheric-pressure plasma jet at successive phases of a 20 kHz applied sinusoidal voltage. The capillary is open to ambient air, and a neon gas stream is directed from right to left. [41]

The direction and velocity of plasma fronts are also influenced by polarity. Downstream bullets, propagating outward into the atmosphere, consistently exhibit higher velocities than upstream bullets that occasionally propagate backward into the device. For example, downstream bullets in helium or neon jets have been measured with velocities up to 30 km/s, whereas upstream bullets typically remain below 1 km/s [40, 41].

Another important factor is the design of the electrode surface. Sharp edges or points lead to local field intensification, which promotes uncontrolled corona discharges or flashovers [42]. For this reason, electrodes for DBD jets are manufactured with smooth, rounded surfaces to ensure uniform field distribution.

Overall, electrode design governs where the discharge ignites, how the plasma bullets form, and how far the jet propagates into the ambient atmosphere. By tailoring electrode geometry, placement, and polarity, the plasma jet properties can be optimized for applications ranging from localized surface processing to biomedical treatments.

4 Methodology

The objective of the methodological approach was to systematically investigate the individual components of the system and their interaction. In the first step, the existing levitation setup was analyzed and its functionality documented. Subsequently, plasma behavior was examined using a DBD configuration based on the design in Figure 3.7 [39]. In the final step, the plasma source and the levitation module were experimentally combined to identify potential interactions and operational limitations

Figure 4.1 illustrates the overall investigation process. The development is structured into three consecutive phases, each characterized by targeted experimental series and directly contributing to the final reactor configuration.

Figure 4.1: Structured investigation process for the development of a combined plasma–levitation reactor. The process is divided into three consecutive phases: (1) characterization of the plasma system in standalone operation, (2) integration with the levitator under realistic conditions, and (3) derivation of the final reactor configuration. Each phase builds upon the findings of the previous one.

4.1 Characterization of the existing ADL System

As part of this project, it was specified to use the existing aerodynamic levitation (ADL) system of the German Aerospace Center (DLR) as the experimental basis [28]. The objective was to extend this system in such a way that it would enable crucible-free treatment of levitated samples using atmospheric-pressure plasmas. To prepare this integration in a structured and technically sound manner, a detailed analysis of the existing levitation setup was first required. The experimental system can be functionally divided into four main components: the levitation unit, the heating system, the diagnostic equipment, and the process chamber. The description of these components forms the foundation for the subsequent implementation of the plasma module. An overview of the complete setup is provided in Figure 4.2.

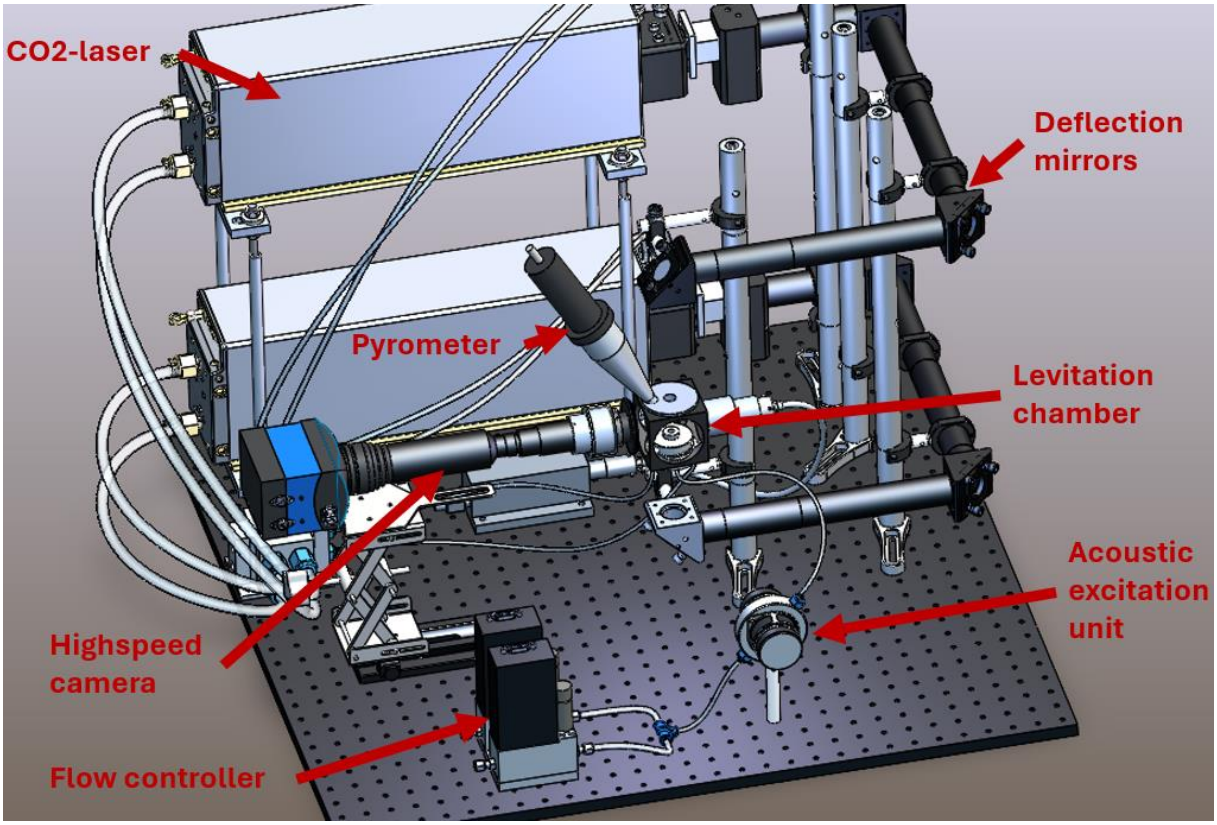

Figure 4.2: CAD model of the existing levitation system at DLR. Shown are the two CO_2 lasers with deflection mirrors, the central levitation chamber with attached nozzle, the high-speed camera positioned on the left, and the fiber-coupled pyrometer mounted above the chamber.[43]

4.1.1 Levitation Unit

The core component of the existing system is the levitation unit. It consists of a modular nozzle body that integrates the gas nozzle, inlet fittings, and a water-cooling system. The nozzle itself is exchangeable and designed to generate a vertically directed gas jet that stabilizes samples in mid-air. The entire assembly is mounted inside the process chamber and can be vertically adjusted to ensure precise alignment with the focal region of the heating lasers and the diagnostic optics. [43]

Gas is supplied via two independently controllable lines, each regulated by electronic mass flow controllers with a maximum flow rate of 2l/min (see Figure 4.2). This allows for a flexible gas composition. Typically, either pure argon or an argon–oxygen mixture is used, both of which enable stable levitation. Before entering the nozzle, the gas flow passes through an acoustic excitation unit consisting of two opposing loudspeakers (see Figure 4.2). These induce controlled mechanical oscillations in the gas stream, which in turn excite specific vibrational modes in the levitated liquid droplet. This mechanism is particularly relevant for subsequent viscosity measurements, where mode-specific damping behavior is analyzed. [43]

To protect the nozzle from thermal stress during laser heating, the nozzle body includes an integrated water-cooling loop. Cooling fluid is circulated through a ring-shaped internal channel, which maintains a constant temperature across the entire nozzle geometry (Figure 4.3b). The design includes four evenly distributed inlet/outlet ports, ensuring homogeneous thermal conditions during extended operation. [43]

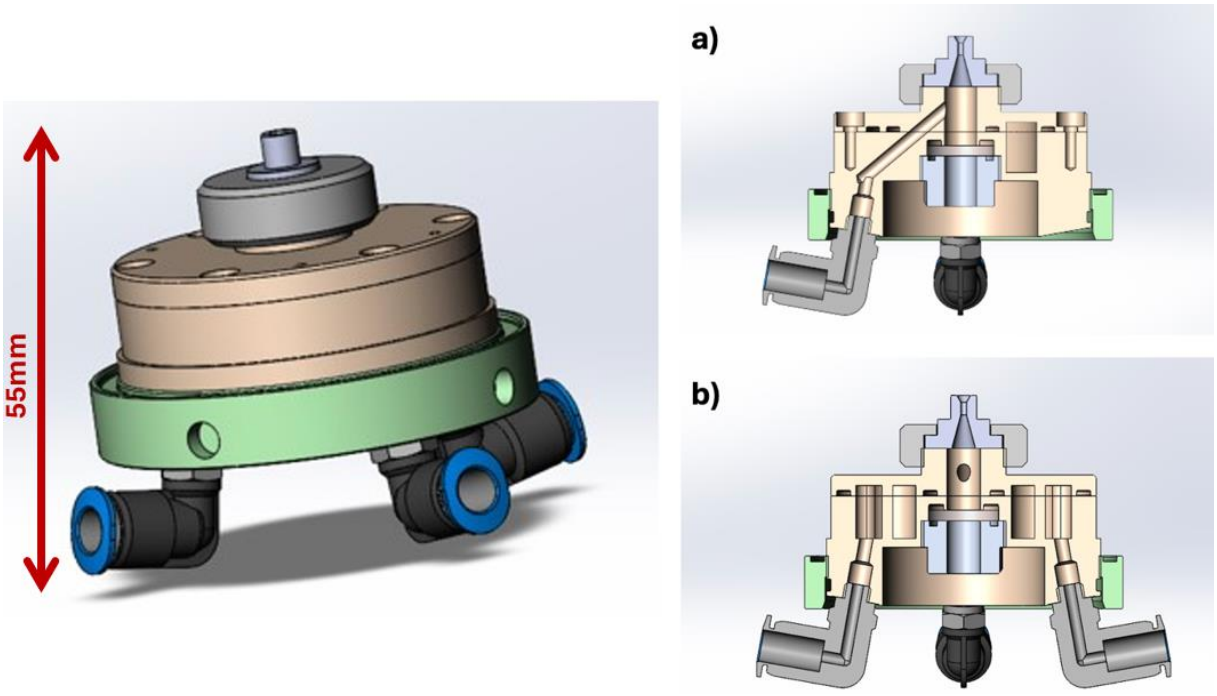

Figure 4.3: CAD view of the nozzle used in the levitator. a) Section view showing the gas flow path, b) Section view highlighting the integrated water-cooling channel.

The levitation chamber itself is sealed and optimized for laminar, undisturbed flow conditions. This not only ensures process stability during levitation but also prevents contamination by ambient air. The modular design of the nozzle unit allows for quick reconfiguration, for example when switching between different nozzle geometries or integrating additional components. [43]

4.1.2 Heating System

Controlled heating of the levitated sample is achieved using a dual CO_2 laser setup. The two laser beams are arranged vertically, irradiating the levitation zone from above and below. This configuration enables a nearly homogeneous temperature distribution within the mm-sized sample, which is essential for conducting targeted investigations under isothermal conditions. [43]

Each laser beam has a maximum power of approximately 30 W at a wavelength of 10.6 µm and is guided into the system via three deflection mirrors. The mirrors are mounted on holders that allow precise two-axis adjustment. Gold-coated copper mirrors are used due to their high reflectivity in the infrared range and thermal resistance. Focusing mirrors are employed in the final stage of the beam path to concentrate the laser power precisely into the center of the levitation zone, ensuring symmetrical energy input. [43]

The lower laser beam passes through the nozzle via an infrared-transparent sodium chloride (NaCl) window. This window is flush-mounted into the nozzle geometry, allowing low-loss transmission of the IR radiation while simultaneously sealing the gas volume. As a result, the sample can be efficiently heated from below without disturbing the levitation flow. [43]

For alignment purposes, each laser is equipped with a visible diode laser that is coupled into the beam path via a mirror system. These pilot beams are used for alignment purposes. Power control of the CO_2 lasers is achieved via UC2000 controllers, which are regulated through a

0–10 V analog signal. The laser system is fully integrated into the central LabVIEW control environment, allowing both manual and automated power profiles. [43]

During the experiment, the laser powers are typically set asymmetrically. This compensates the cooling effect of the gas flow and ensures that the entire sample is uniformly heated to the molten state. The typical heating phase proceeds continuously until the target temperature is reached, as monitored by the pyrometer system. [43]

4.1.3 Diagnostics

The behavior of the levitated droplet is analyzed using a combination of imaging and thermal diagnostics. The objective is to monitor the droplet's shape, position, and motion, as well as its thermal evolution during both the heating and cooling phases.

Optical imaging is performed using a high-speed camera positioned laterally to the levitation zone. The camera is mounted on an adjustable rail system, allowing fine control of height and distance relative to the sample. A telecentric lens is used to ensure a constant image scale, independent of minor positional changes. This is particularly important for quantitative image evaluation during oscillation or drift of the droplet. [43]

To improve image contrast, a backlighting shadowgraph technique is employed. A 660 nm diode laser provides collimated background illumination, while a bandpass filter matched to the laser wavelength is placed in front of the camera. This configuration suppresses the self-emission of the hot sample in the visible spectrum, enabling accurate contour detection regardless of temperature. The resulting high-contrast silhouettes are ideal for geometric analysis. [43]

Temperature measurements are conducted using a fiber-optically coupled pyrometer that is positioned at an inclined angle above the levitation zone. The pyrometer is aligned to capture the largest possible emission area, improving the reliability of the measurement. Assuming a constant emissivity, systematic errors can be minimized through prior calibration. [43]

The combined image and temperature data are used to quantitatively characterize the droplet behavior throughout the experiment. In particular, the video recordings are analyzed for geometric parameters such as droplet radii, oscillation modes, and damping behavior, while the pyrometer provides continuous temperature monitoring. [43]

4.1.4 Process Chamber

The levitation unit is enclosed in a process chamber designed for experiments under controlled environmental conditions. The chamber (at least, to some extent) provides a defined atmosphere, minimizes flow disturbances, and maintains optical access for diagnostic systems (see Figure 4.4).

It consists of a cube.shaped stainless-steel housing with multiple lateral and vertical ports. These ports accommodate the nozzle unit, gas lines, optical components, and sensors. A central top opening allows the installation of the pyrometer. Side windows made of quartz or infrared-transparent materials enable camera and laser access.

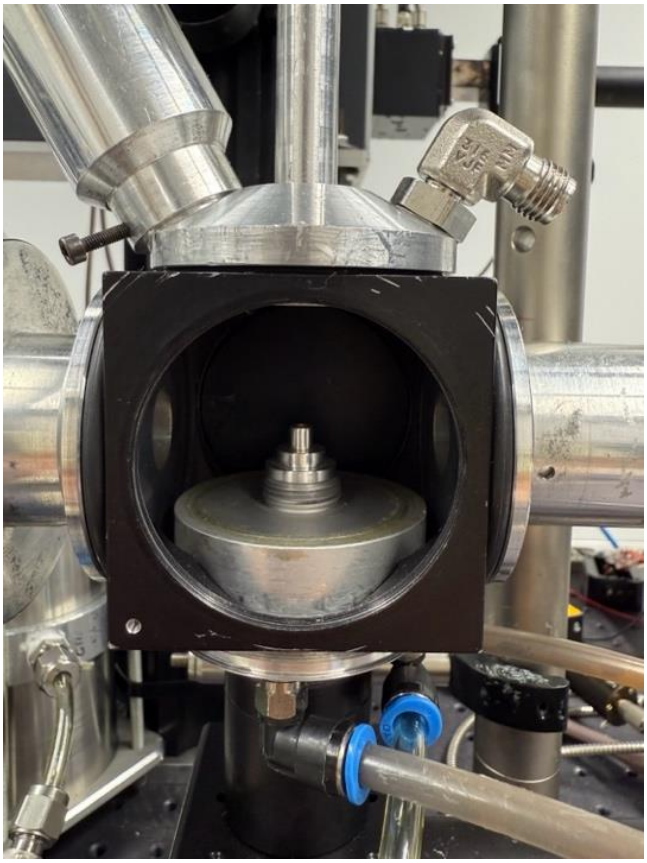

Figure 4.4: View inside the Process Chamber (Thorlabs cube)

Sealing is achieved using O-rings made of temperature- and chemical-resistant materials. This ensures that the levitation gas is directed through the nozzle and protects the system from external turbulence. The chamber allows stable and reproducible atmospheric conditions, even with varying gas compositions.

The chamber is mounted on a vertically adjustable experimental frame. This enables precise alignment of the optical axes and flexible adaptation to different test setups. An internal LED light source supports visual inspection during alignment and sample placement.

The modular design permits easy access to all functional components. This facilitates maintenance, system modifications, and integration of additional measurement devices such as the later plasma module. Figure 4.5 provides an overview of the essential components of the ADL system in a clear schematic representation.

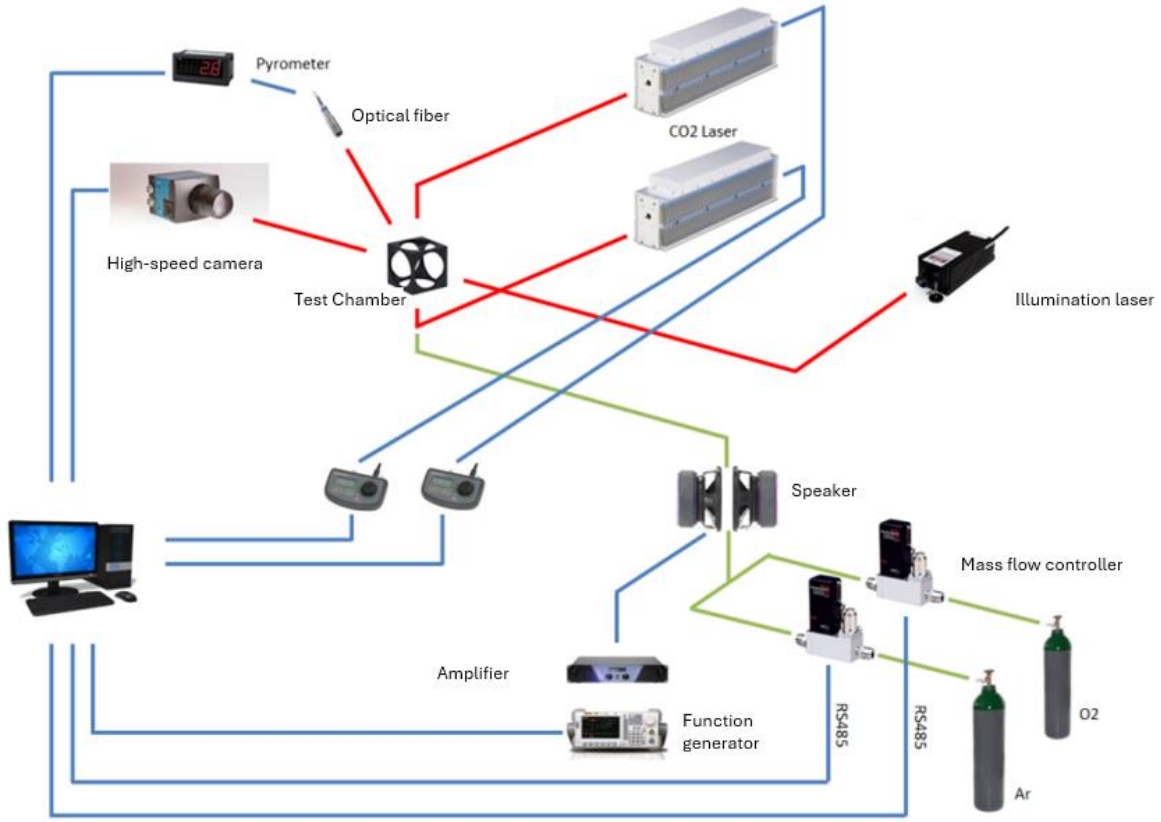

Figure 4.5: Schematic overview of the essential components of the ADL system. The color coding highlights different functional groups: red indicates the diagnostic instruments, green the gas supply components, and blue the control elements. [43]

4.2 Experimental Analysis of Plasma Behavior

To analyze the behavior of a dielectric barrier discharge (DBD) plasma jet at atmospheric pressure, an experimental setup (see Figure 4.6) was implemented based on the concept in Figure 3.7. [39]. The objective was to investigate key plasma parameters such as ignition behavior, discharge stability, jet direction, and thermal load. The findings serve as the basis for the later integration of the plasma system into the levitation setup.

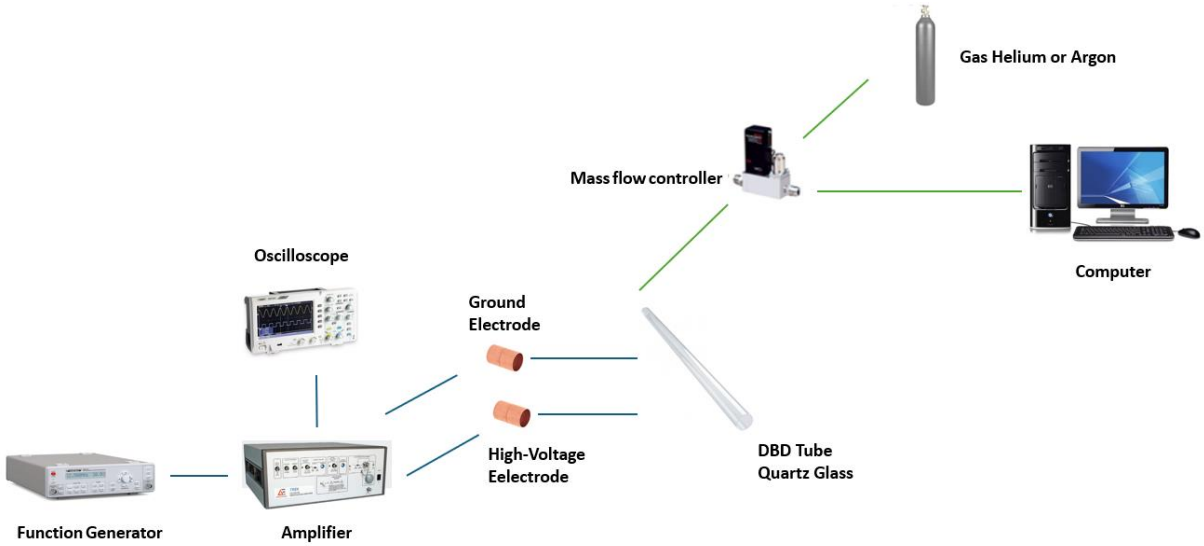

Figure 4.6: Schematic overview of the test setup. Green indicates the units for gas flow control, while blue indicates the units for voltage and frequency adjustment and monitoring.

The core element of the setup was a quartz tube with an outer diameter of 6 mm and an inner diameter of approximately 4 mm. Two ring-shaped copper electrodes were mounted externally on the tube. One electrode was connected to a high-voltage source, while the other was initially grounded. This configuration allowed lateral electrical excitation of the gas through the dielectric barrier.

The high-voltage supply was provided by a TREK 10/10B-HS amplifier, driven by sinusoidal signals from a HAMEG HM8150 function generator operating in the frequency range from 1 kHz to 20 kHz. The amplifier has a voltage gain of 1 V to 1000 V. Frequency and voltage amplitude were verified using an oscilloscope. The setup is shown in Figure 4.6 and 4.7.

Gas flow was controlled by an electronic mass flow controller with a maximum flow rate of 2 l/min. It was connected to the control system of the levitator.

This setup was used to systematically study the plasma ignition conditions as a function of frequency, voltage, gas flow rate, and gas type (Section 4.2.1). In addition, various electrode geometries and spacing were tested to evaluate their influence on discharge formation, luminous intensity, and the occurrence of edge phenomena such as arcing (Section 4.2.2). Finally, the influence of different nozzle geometries on the plasma jet shape and propagation was examined, with particular attention to the electrical coupling between the plasma and the nozzle (Section 4.2.3).

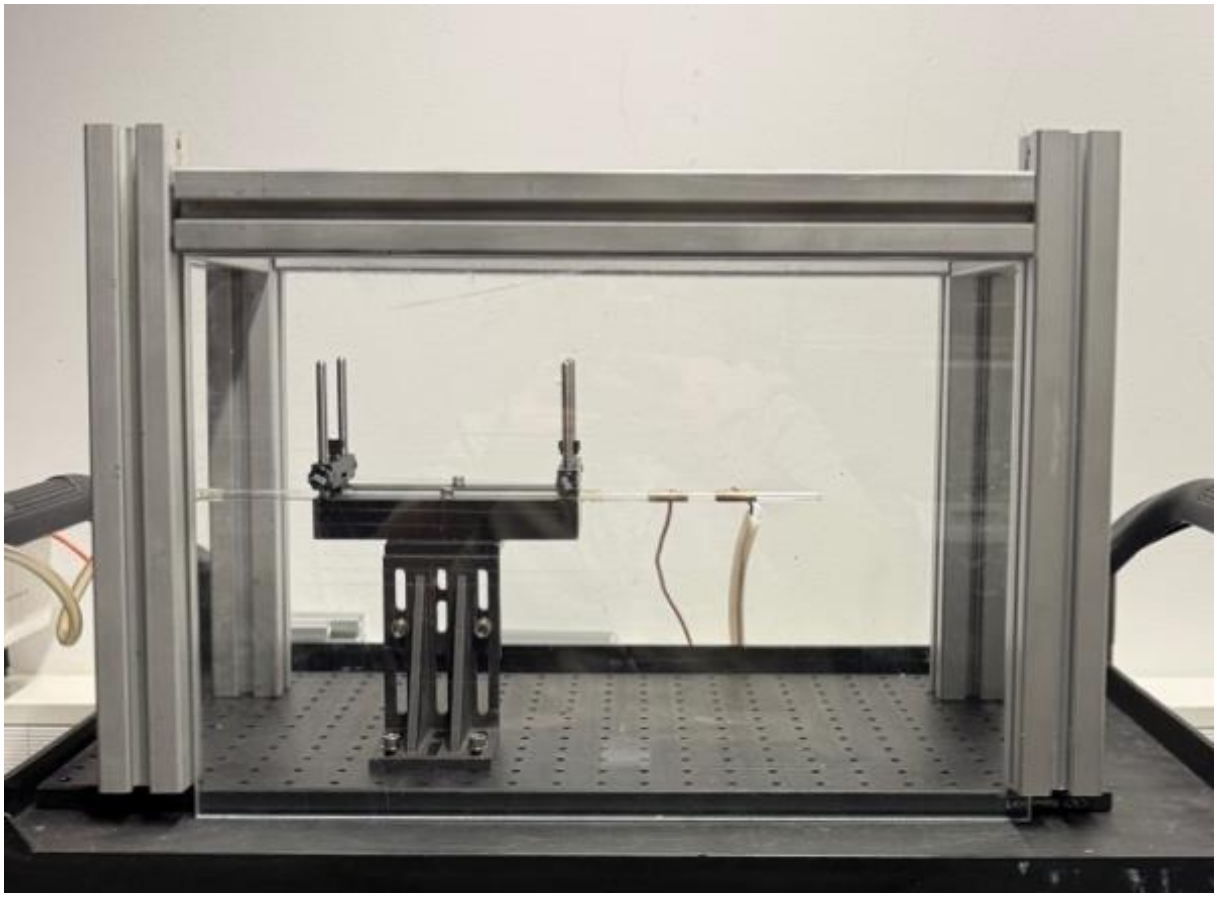

Figure 4.7: Experimental setup for ignition and characterization of the DBD plasma jet. The quartz tube surrounded by two copper electrodes, arranged from left to right as grounded electrode and high-voltage electrode, is mounted in the test frame.

4.2.1 Influence of Operating Parameters on Ignition Behavior

The experimental investigation of the ignition behavior of the dielectric barrier discharge (DBD) plasma jet was conducted under constant conditions. The gas flow rate was fixed at 0.4 l/min throughout all tests, corresponding to the operational requirements of the levitation system (see Section 4.1.1). The electrode spacing was set to a constant value of 2 cm to ensure reproducibility and comparability across all measurements.

The frequency was varied between 1 kHz and 30 kHz, and the output voltage could be adjusted up to approximately 20 kVpp. Signal frequency and amplitude were monitored via an oscilloscope throughout the experiments.

As a starting point, the initial conditions reported by Teschke et al. [39] were applied (13 kHz, 7 kVpp). From this baseline, the frequency was gradually increased and decreased while maintaining constant voltage to determine whether ignition occurred. If a discharge was observed, the respective frequency range was further examined to identify the boundaries of stable operation.

If no ignition occurred at a given voltage level despite frequency variation, the voltage was increased in steps and the frequency sweep was repeated. Conversely, at fixed frequency, the voltage was also gradually reduced to determine the lower ignition threshold. This process was repeated iteratively until the relevant parameter space was mapped.

All tests were conducted with both argon and helium as process gases. The experimental setup remained unchanged to allow a direct comparison of the ignition behavior under otherwise identical conditions. A quantitative evaluation of the ignition regimes is presented in Chapter 5.

4.2.2 Variation of Electrode Spacing and Configuration

To investigate the influence of electrode spacing and configuration on the behavior of the DBD plasma, a series of targeted modifications were made to the experimental setup (Figure 4.7). The aim was to examine the jet direction as a function of polarity and plasma jet length under different electrode spacings.

Initially, ring-shaped electrodes were realized by wrapping adhesive copper tape directly around the quartz tube. High-voltage and ground connections were applied via soldering. However, this method proved impractical due to the time-consuming nature of repositioning the electrodes and the influence of sharp soldered edges on the discharge behavior. As an alternative, cylindrical copper sleeves with a length of 1 cm and an inner radius slightly larger than the 6 mm outer diameter of the quartz tube were fabricated. These sleeves could be slid into position and securely held in place without additional fixation, allowing for precise and reproducible spacing adjustments.

During the experiments, the plasma was first ignited within the stable operational range identified in Section 4.2.1. Then, the electrode spacing was varied step by step, while frequency and voltage were kept constant to ensure comparability in evaluating the changes in plasma jet length.

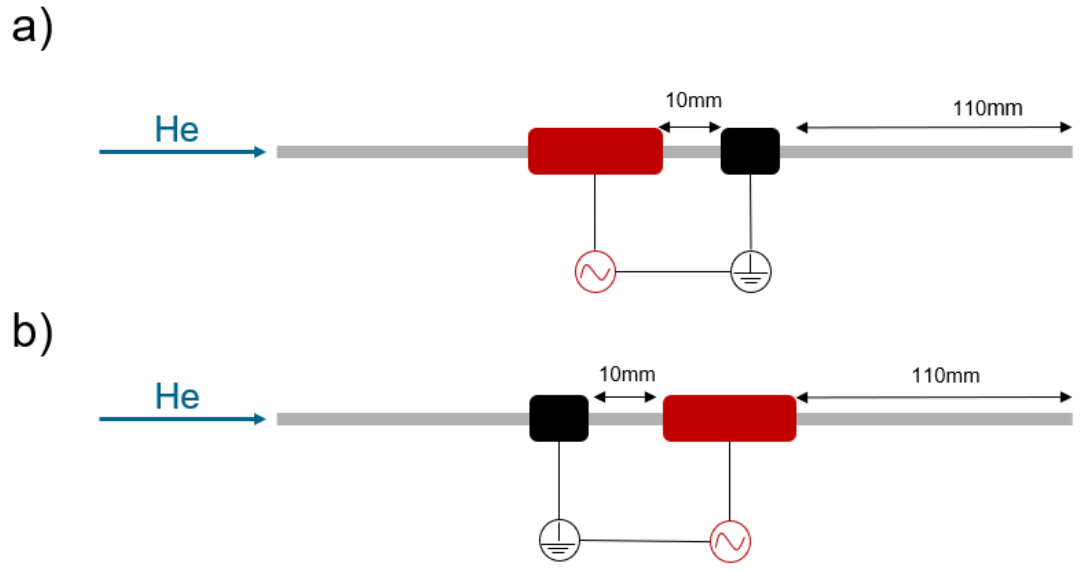

Figure 4.8: Electrode configurations to analyze jet deflection in the DBD quartz tube with helium (HE) flow. (a) High-voltage electrode on the left and ground electrode on the right. (b) Ground electrode on the left and high-voltage electrode on the right. The electrode spacing is 20 mm with a remaining tube length of 110 mm.

In a separate test series, the influence of polarity was analyzed. For this, the high-voltage and ground connections were swapped at a fixed electrode spacing of 2 cm (see Figure 4.8). The orientation of the plasma jet was observed to determine whether a directional change occurred,

as reported in the literature [39]. All experiments were documented through video and photographic recordings.

4.2.3 Influence of Nozzle Geometry on Plasma Behavior

In the final step of the experimental series, it was investigated whether the generated plasma jet could pass through the nozzle of the levitator and how different electrical configurations of the nozzle influenced this behavior. The aim was to systematically analyze the electrical coupling between the plasma source and the nozzle.

The experimental setup shown in Figure 4.7 was also used as the basis in this case and was extended by a nozzle mounted at the right end of the tube, positioned directly downstream of the high-voltage electrode at a distance of about 1 to 2 cm. The electrode spacing was kept constant at 4 cm in all configurations.

For the initial tests, the metallic aluminum nozzle with an exit radius between 1.1 mm and 1.2 mm from the levitation system was used. It was mechanically adapted to the quartz tube using a copper sleeve and fixed in place with heat-resistant adhesive. Three electrical configurations of the nozzle were examined: grounded, electrically floating and high-voltage-powered. In the first two cases (grounded and floating configurations), the two electrodes were used in combination with the nozzle at the tube outlet. In the latter case (high-voltage-powered), no additional electrodes were used; only the nozzle itself was connected via a high-voltage lead to evaluate the effect of localized high-voltage excitation.

Additionally, another nozzle was 3D printed out of polylactic acid (PLA) keeping the essential dimension of the original design. The resulting plastic nozzle is shown in Figure 4.9.

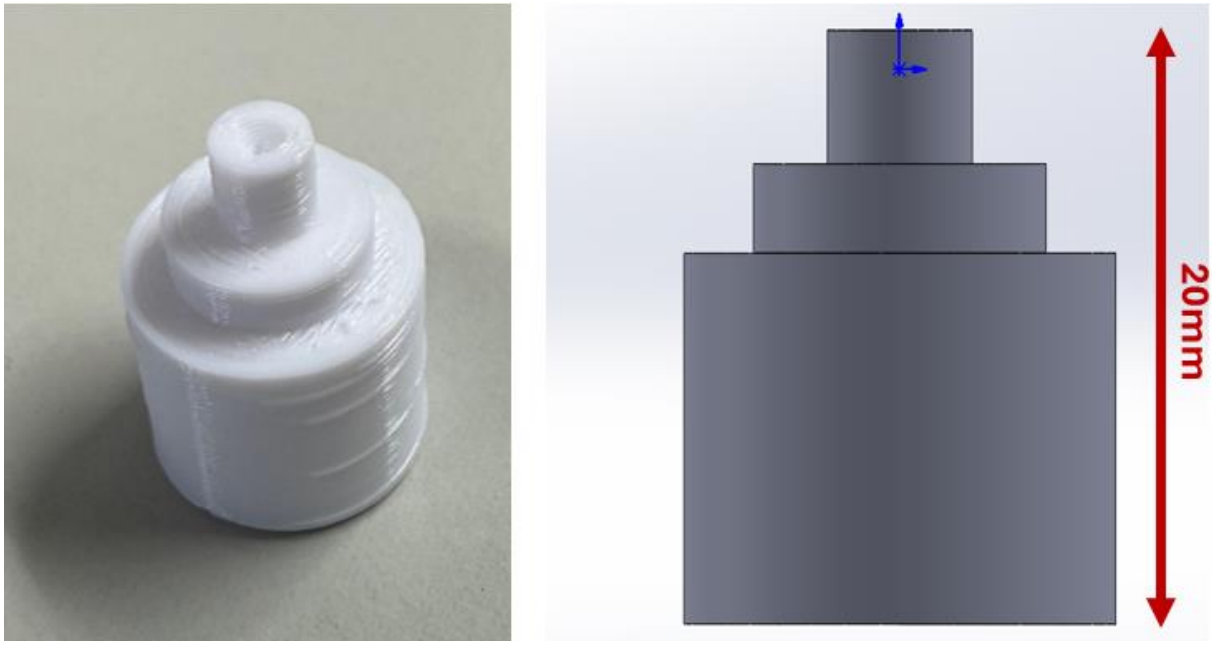

Figure 4.9: 3D-printed nozzle made of polylactic acid (PLA), manufactured to enable an electrically insulating configuration. The design is based on the design of the original aluminum nozzle of the levitation system.

All tests were conducted under constant ignition conditions as described in Section 4.2.1. After attaching each nozzle to the tube, it was observed whether a stable plasma jet penetrated trough the nozzle opening. To improve visibility of the plasma jet, the gas flow rate was gradually increased while all other parameters remained unchanged.

4.3 Experimental Investigation of the Coupled Plasma-Levitation System

Following the separate investigations of the levitation system and the plasma behavior in the previous sections, the next step involved the experimental integration of both subsystems. The objective of this coupling was to integrate the plasma jet directly into the existing nozzle body of the levitation chamber. Three central questions were addressed during this experimental phase:

(i) Is stable plasma ignition possible under real conditions inside the levitation chamber?
(ii) Can plasma jet propagate through the nozzle and enter the levitation field?
(iii) Can the levitated sample be reached by the jet, allowing for a direct interaction between the plasma and the sample surface.

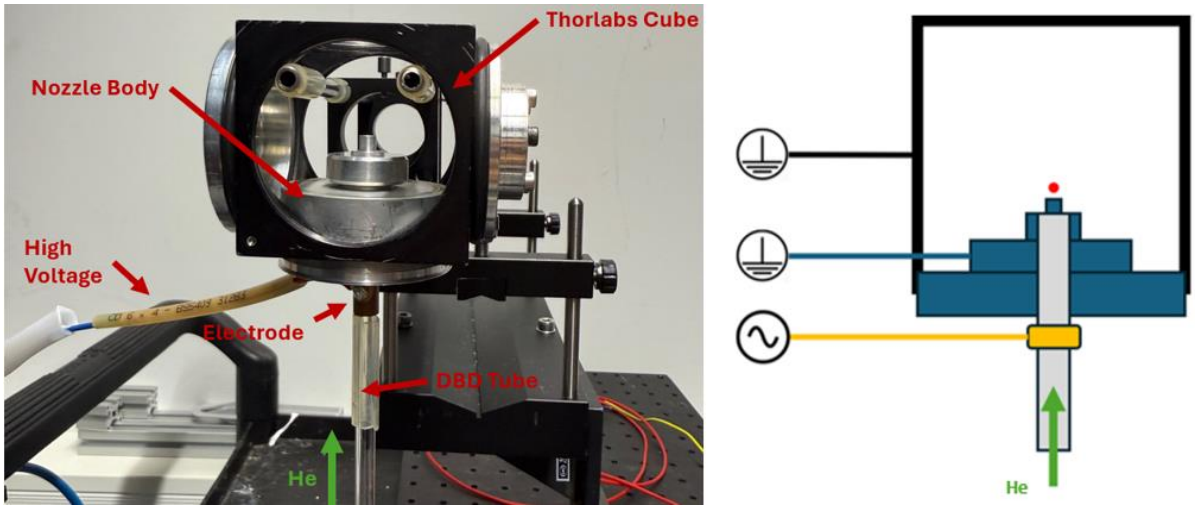

Figure 4.10:. Integration of the plasma unit and the levitation unit. Left: Photograph of the experimental setup. The quartz tube, equipped with a high-voltage electrode, is inserted into the central nozzle channel, with gas flow introduced from below. The aluminum nozzle is mounted at the outlet to mimic real operating conditions. Right: Schematic illustration of the same configuration, showing the electrical connections, the gas flow through the nozzle, and the levitated sample sphere.

At the time of testing, the original levitation setup was in use, which necessitated the implementation of the combined system on a dedicated model assembly. For this purpose, the entire nozzle unit, including the aluminum nozzle and the Thorlabs mounting cube, was mounted on an optical table. The quartz tube was inserted into the central channel of the nozzle block, which normally serves as the passage for the lower heating laser described in Section 4.1.2. With an inner diameter of 6.1 mm, the channel provided a precise fit for the quartz tube. A high-voltage electrode was mounted on the outer surface of the tube, and the assembly was positioned vertically so that the tube was inserted up to the mechanical contact with the nozzle opening (see Figure 4.10). The gas supply was connected at the lower end of the quartz tube, allowing for axial flow from bottom to top.

Plasma ignition was carried out using the same signal parameters identified in Section 4.2.1. The initial gas flow rate was set to 0.4 l/min to match the operational conditions of the levitation system. Due to minor leakages in the model, the flow rate was increased up to 2 l/min in some trials to ensure visible jet formation.

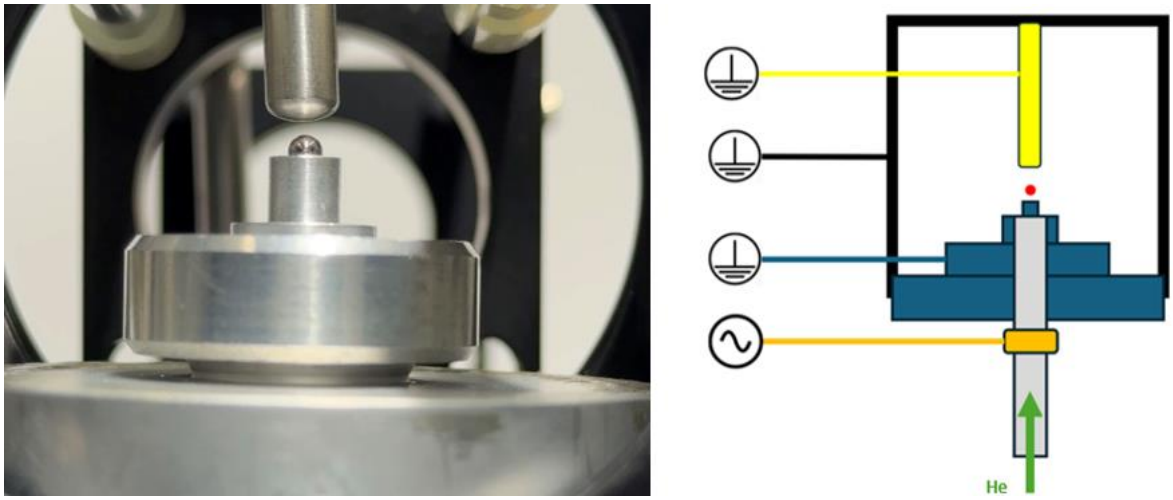

Figure 4.11: Frontal view of the levitation chamber with an integrated grounded rod electrode positioned above the nozzle. This configuration was used to investigate the influence of a counter-electrode on plasma propagation and its interaction with the levitated sample.

For the levitation trials, a 2.5 mm diameter aluminum sphere was used. To evaluate different coupling configurations and electrical conditions, the setup was modified in several ways. In one modification, a rod electrode connected to ground potential was mounted directly above the nozzle orifice to guide the electric field lines and enhance discharge stability (Figure 4.11). In another configuration, the entire nozzle assembly was redesigned in CAD and 3D printed out of PLA. This approach enabled a completely electrically insulating nozzle geometry (Figure 4.12).

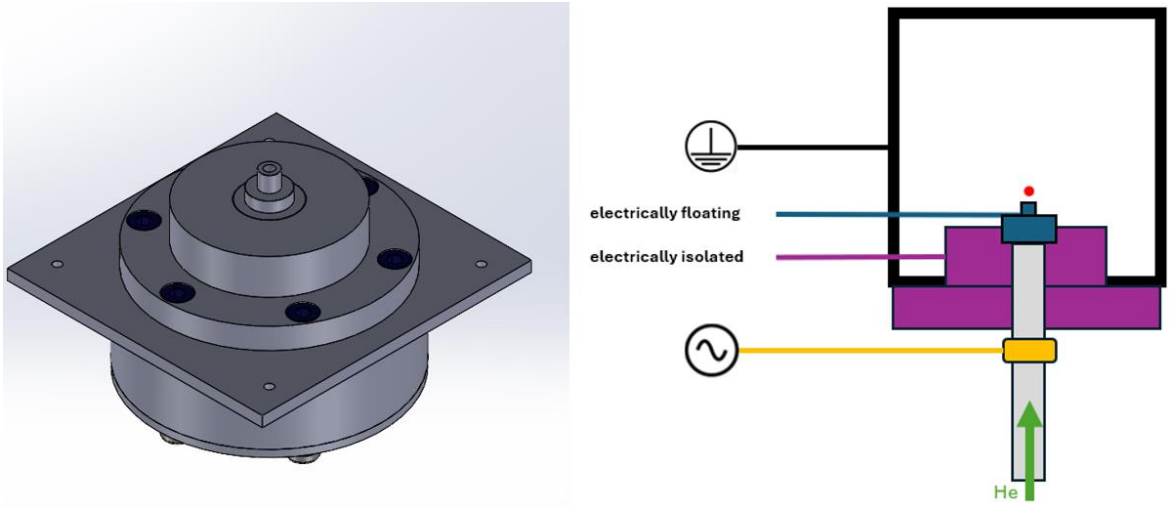

Figure 4.12: CAD model of the fully 3D-printed nozzle holder made of electrically non-conductive PLA. This version was developed to enable complete electrical decoupling between the nozzle and ground potential.

The results of these integration tests provided key insights and are presented in detail in Chapter 5, where they are discussed in the context of deriving the final reactor design.

5 Results and Discussion

This chapter presents the experimental results and interprets them in relation to the theoretical considerations outlined in Chapter 3. In addition, the step-by-step development of a reactor is described, based on the experimental findings. The reactor enables the combined operation of a plasma jet and sample levitation within an integrated setup. The results are evaluated systematically and used to derive a consistent design.

5.1 Results of the Plasma Experiments

The experimental investigation focused on the behavior of the plasma under varying boundary conditions. Particular attention was given to the ignition characteristics of different noble gases, the influence of electrode configuration, and the interaction between the plasma jet and selected nozzle geometries. The insights gained from these analyses served as the basis for defining suitable operating parameters and enabled the stable integration of the plasma unit into the aerodynamic levitator system.

5.1.1 Ignition Behavior of Argon and Helium

To identify suitable operating parameters for plasma ignition, systematic experiments were conducted using argon and helium as process gases. The experimental setup is described in Section 4.1.

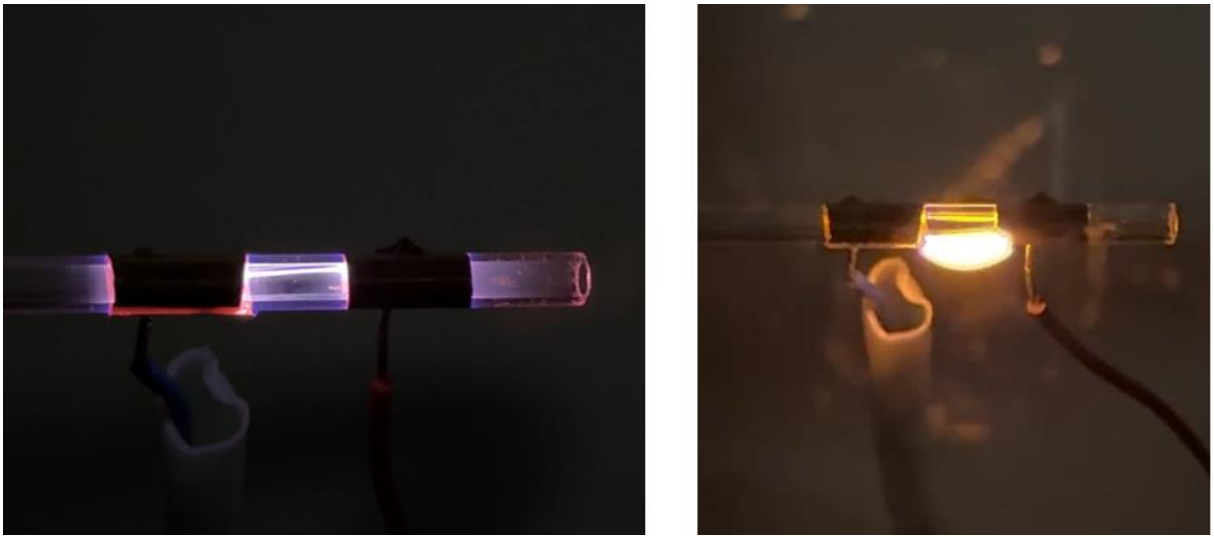

Figure 5.1: Unstable discharge formation in argon. On the left, the plasma appears as transient, filamentary structures along the electrode region, fluctuating from pulse to pulse and indicating strong temporal and spatial instability. On the right, this unstable behavior develops further into arcing outside the gas flow channel.

When using argon, ignition was observed only at a peak voltage of approximately 19 kVpp. The discharge appeared as filamentary channels along the inner wall of the quartz tube (Fig. 5.1). As the voltage increased, arcing occurred between the electrodes on the outer side of the tube, accompanied by visible material erosion at the electrode edges (Fig. 5.1). A stable,

flicker-free glow discharge could not be achieved under the given conditions. Despite varying the excitation frequency in the range of 1 to 30 kHz, the plasma exhibited strongly fluctuating and unstable behavior.

In contrast, helium enabled a stable discharge at approximately 7 kVpp and frequencies above 10 kHz. Within the optimal range of 10 to 13 kHz and 15 to 17 kVpp, a homogeneous and continuously glowing plasma zone formed along the copper electrodes (Fig. 5.2). The plasma remained calm and uniform throughout this range. Outside these parameters, particularly at higher voltages or lower frequencies, bundled filaments reappeared, accompanied by noticeable heating of the quartz tube.

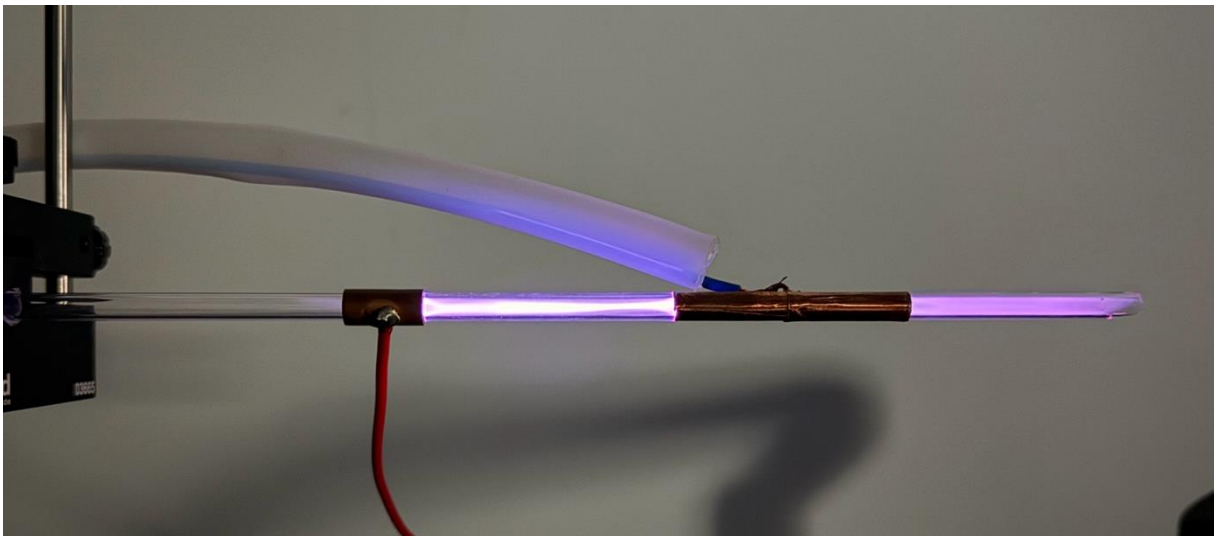

Figure 5.2: Stable helium plasma discharge at 13 kHz and ~16 kVpp, forming a homogeneous, luminous zone across the copper electrodes.

The observed differences in ignition behavior can be explained by the lower breakdown voltage of helium compared to argon. Figure 5.3 from Chen et al. [44] shows that helium requires significantly less breakdown voltage than argon, nitrogen, or oxygen, primarily because helium electrons lose less energy before ionization. This accelerates the ionization process and facilitates the establishment of a stable glow discharge. These findings are consistent with our experiments, where helium enabled reliable ignition at considerably lower voltages and gas flow rates. [44]

The results are further supported by Javanmard and Pouryoussefi [45], who showed that helium, under identical operating conditions, generates a more uniform, stable, and thermally moderate plasma. In contrast, argon requires either significantly increased gas flow rates or higher electrical power input to achieve a stable discharge. [45] A combination of high voltages and high flow rates could not be realized in the present work, since the high-voltage generator was limited to a maximum of 20 kVpp and the gas flow rate to 2 L/min. Higher flow rates would not satisfy the aerodynamic levitation condition.

Helium, on the other hand, enabled reliable ignition and the formation of a stable plasma zone even at considerably lower voltages and gas flow rates. These properties make it the preferred process gas for the intended reactor operation, particularly under the given boundary conditions.

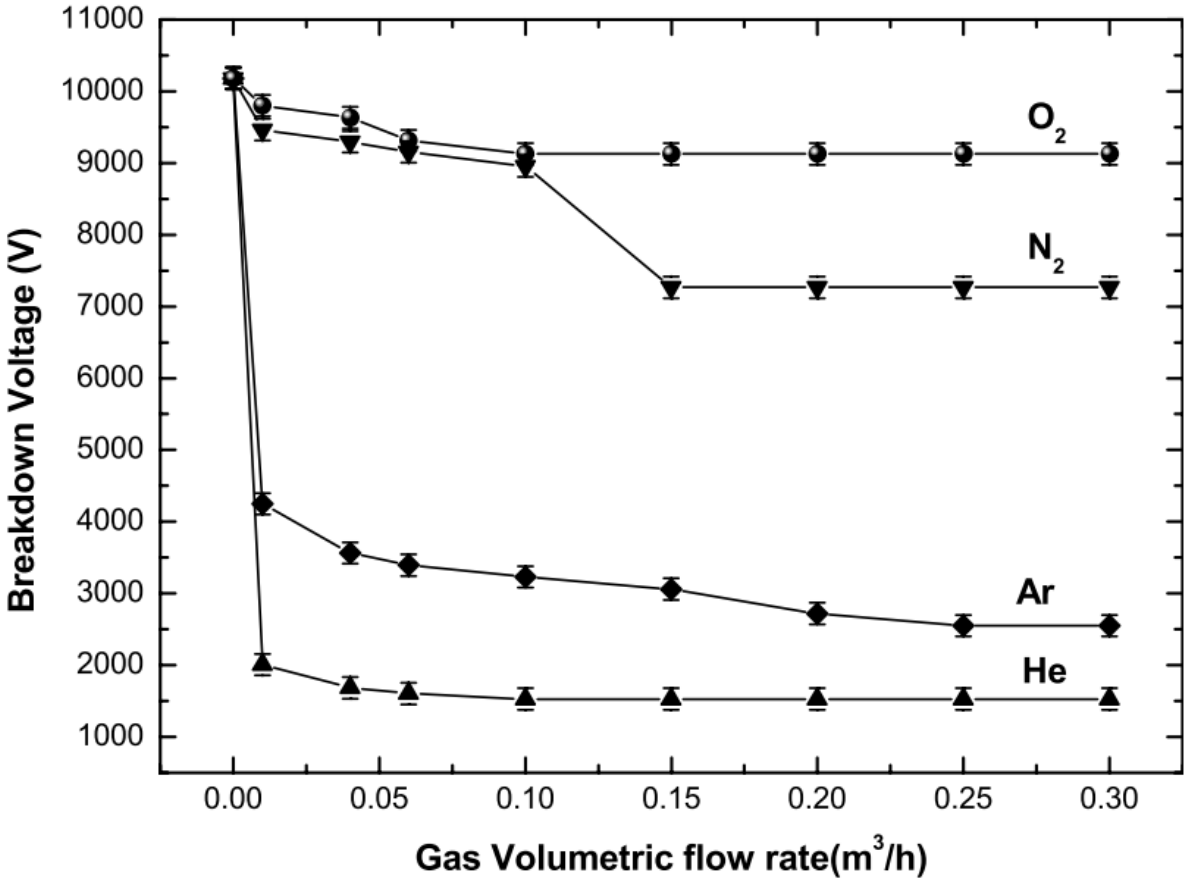

Figure 5.3: Breakdown voltage measured in He, Ar, N_2, and O_2 at 8.4 kHz with an outer electrode conductivity of 0.11 S cm^{-1}. [44]

It should be noted, however, that the present experiments were carried out exclusively with pure helium. In the final reactor design, a helium-hydrogen gas mixture with 2% H_2 is intended for use. This mixture was not available at the time of testing. Since hydrogen increases the electrical conductivity of the plasma, it is expected that the ignition conditions may shift slightly, potentially requiring somewhat higher voltages. Experimental validation of this assumption is still pending.

5.1.2 Influence of Electrode Configuration and Geometry

After identifying the stable operating range for helium between 10 and 13 kHz at voltages of 15–17 kVpp and a flow rate of 0.4 L/min, systematic investigations were carried out to evaluate the influence of electrode spacing, polarity and geometry. To ensure comparability, all tests were conducted under constant excitation conditions of 17 kVpp and 11 kHz.

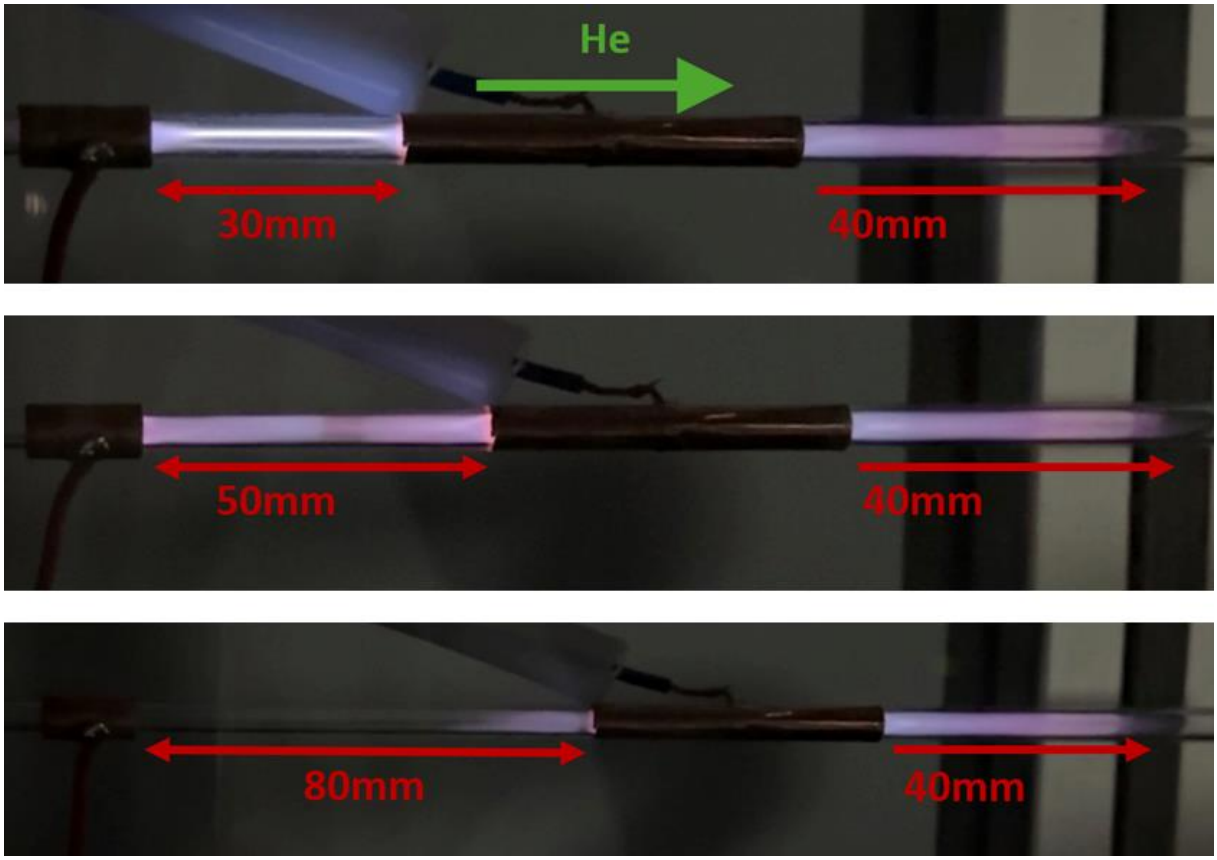

Figure 5.4: Electrode gap variation from 3 cm to 8 cm (15 kVpp, 13 kHz). Plasma ignition occurs reliably in all cases, with no significant change in jet length (40mm).

The results showed that stable discharges were achieved across all tested electrode gaps. Whether the distance was 3 cm, 5 cm or 8 cm, the visible plasma jet length remained nearly unchanged (Figure 5.4). A significant extension of the jet only occurred when the excitation frequency was reduced to 5 kHz and the voltage increased to 20 kVpp (Figure 5.5). This indicates that the discharge behavior is primarily governed by frequency and voltage, while electrode spacing plays a secondary role.

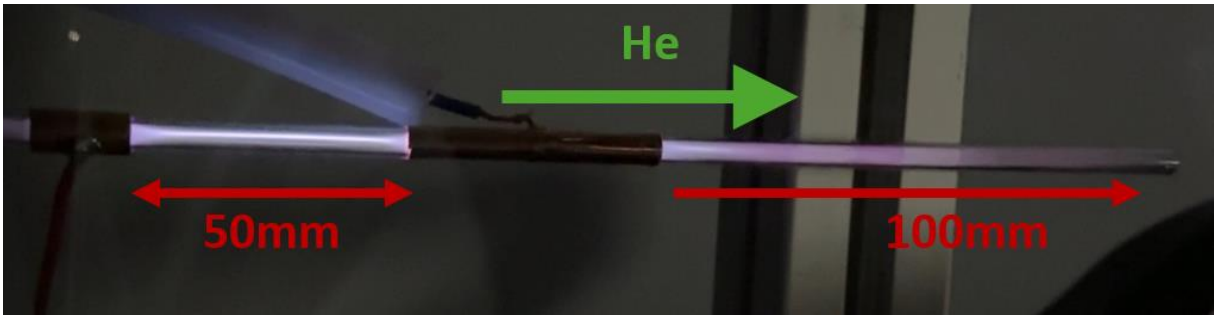

Figure 5.5: Extended plasma jet observed at 5 cm spacing, 5 kHz frequency, and 20 kVpp. The combination of low frequency and high voltage promotes a long and stable discharge.

In tests involving the reversal of electrode configuration, the plasma jet consistently formed from the grounded electrode toward the high-voltage side, even when this direction opposed the gas flow. In Figure 5.6, this behavior is visible in the yellow-circled regions, where the jet deflects more strongly in the direction of the gas stream and appears brighter. In addition, a second, weaker jet was observed propagating in the opposite direction, as highlighted by the

red-circled region in Figure 5.6. However, its intensity was considerably lower and its spatial extension remained limited.

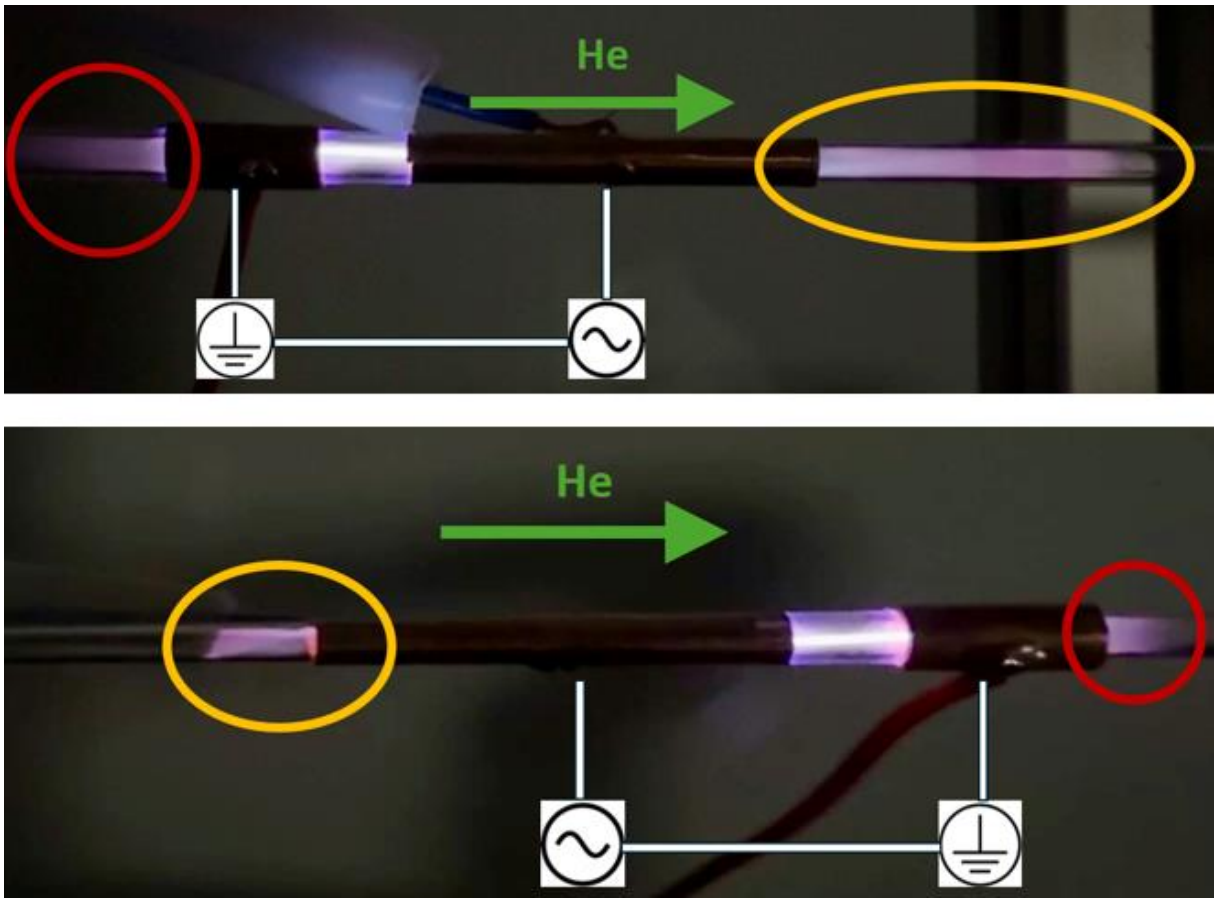

Figure 5.6: Plasma jet propagation with reversed configuration. The images show the influence of electrode configuration on the propagation direction of the plasma jet. The main jet, highlighted in yellow, consistently forms from the grounded electrode toward the high-voltage electrode. This behavior is observed both downstream (top image), where the jet appears brighter and longer, and upstream against the gas flow (bottom image). In addition, a weaker secondary jet propagates in the opposite direction of the main jet, as indicated by the red circles. Its intensity is considerably lower and its spatial extension is limited.

The findings confirm that within the tested range of 3–8 cm, electrode distance does not significantly affect discharge stability or visible jet length, provided that the excitation conditions are kept constant. Variations of frequency and voltage produced a marked influence on jet development. This observation aligns with reports in the literature emphasizing the dominant role of electrical driving parameters in determining the behavior of atmospheric DBD jets. [45]

The clear orientation of the jet from the grounded electrode toward the high-voltage side can be explained by the electric field distribution. Oh et al. [41] report that, depending on the phase of the sinusoidal excitation, discharges can also occur in the opposite direction. During the negative half-wave, the grounded side can act as a relatively higher potential than the HV electrode. Nonetheless, during the positive half-wave, the plasma jet remains more pronounced and stable, particularly when it propagates in the same direction as the gas flow. Therefore, the configuration with gas flow and electrode polarity from ground to HV was determined to be the most effective. [41]

The observed field enhancements at sharp electrode edges caused unstable discharge behavior and thermal stress. These effects highlighted the necessity of optimizing electrode

geometry. A ring electrode with rounded edges was designed to reduce local field intensities and improve spatial symmetry. This geometry enabled a uniform, thermally stable discharge and was thus selected for the final reactor configuration. A technical drawing of this electrode is included in the appendix.

5.1.3 Nozzle integration

The nozzle is one of the most important components of the entire system. Its geometry affects the stability of aerodynamic levitation. At the same time, the nozzle is going to be a part of the plasma channel. To ensure compatibility with the existing levitator module, a proven aluminum nozzle with an outlet diameter of approximately 1.1 mm was selected, as described in Chapter 4.1.1. This allowed the focus to remain entirely on investigating the electrical interaction between the plasma and the nozzle.

Four different electrical configurations were tested: the nozzle was (1) grounded, (2) connected to high voltage, (3) electrically insulating, and (4) floating. In cases 1), 2) and 3), the nozzle was metallic, whereas, in case 3), electrically insulating. All tests were carried out using previously identified optimal plasma parameters: 17 kVpp, 11 kHz, helium, and a flow rate of 0.4 L/min.

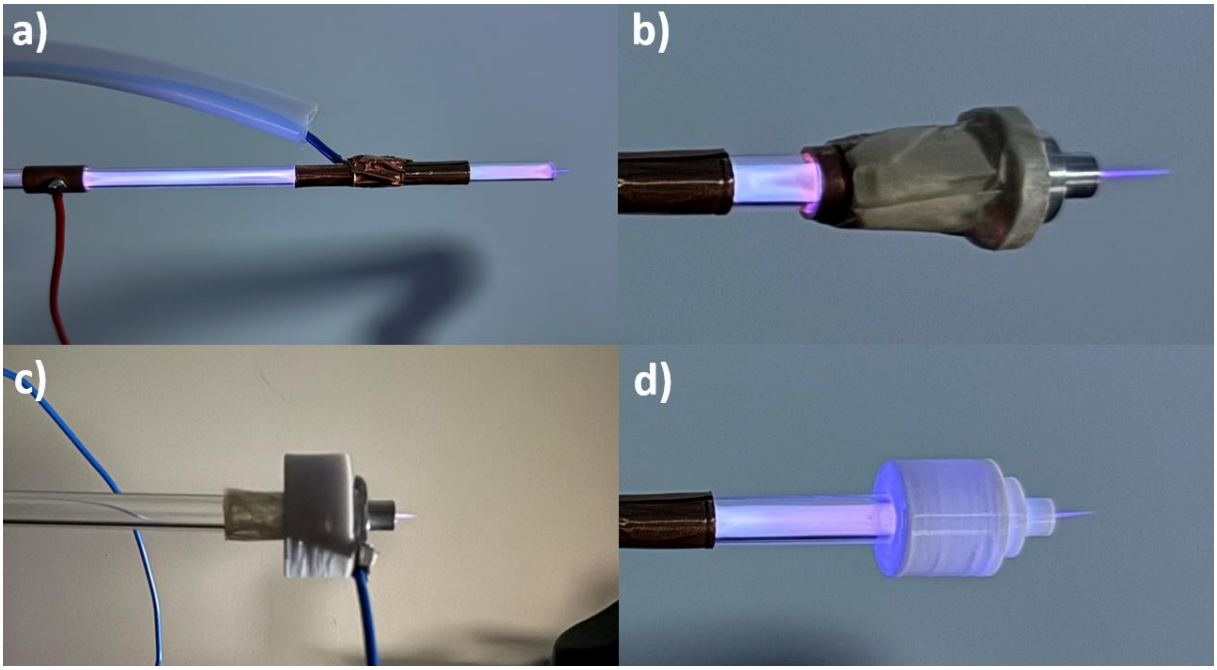

Figure 5.7: Investigated configurations for nozzle coupling. a) Without nozzle, b) metallic nozzle floating, c) metallic nozzle at high voltage, d) electrically insulating nozzle (3D-printed).

In three of the four configurations (floating, high-voltage, and electrically insulated) a stable plasma jet penetrating trough the nozzle (Figure 5.7). Only in the grounded configuration the discharge ended at the transition between the quartz tube and the nozzle, and no visible plasma jet was present behind the nozzle.

The results confirm that a directed propagation of the plasma jet through the nozzle is possible, provided that an appropriate electrical configuration is selected. While connecting the nozzle directly to high voltage appears to be the most straightforward solution from a design

standpoint, this configuration proves unsuitable for the final system. The plasma reactor operates inside a sealed Thorlabs cube that is flooded with helium (see Chapter 4.1.4). Applying high voltage to the nozzle within this environment would result in uncontrolled discharges throughout the interior of the chamber. This would compromise operational stability and interfere with optical diagnostics, making this configuration unusable.

The electrically insulated plastic nozzle, produced by 3D printing, initially showed clean discharge behavior. However, in combination with CO_2 laser heating, this configuration becomes unsuitable, since accidental misalignment of the laser could cause serious damage.

The only technically and functionally viable solution was to operate the existing aluminum nozzle in a floating configuration. In this situation, the plasma jet remained stable and penetrated through the nozzle. At the same time, this solution introduces new challenges for the overall system. These aspects are analyzed in more detail in the following section.

5.2 Analysis of the Coupling Constraints

As described in Chapter 4.1, the aerodynamic levitation system at the institute consists of several functionally interconnected subsystems. The objective of the final reactor design was to primarily modify the levitation unit, while leaving the remaining components unchanged. This approach introduced technical boundary conditions that had to be carefully considered for the integration of the plasma system.

The coupling tests described in Chapter 4.3 were conducted to evaluate the reactor under realistic operating conditions. A key constraint arises from the laser heating setup: As outlined in Section 4.1.2, the levitated sample is heated using two CO_2 lasers, one of which passes axially through the nozzle support body. To implement this geometry, the housing must be manufactured out of a metallic material. In addition, the thermal load introduced by the laser requires active water cooling in this area to ensure the thermal stability of the nozzle.

Another important boundary condition is the use of the process chamber. As discussed in Section 4.1.4, this chamber forms the interface between the levitation unit, laser systems and optical diagnostics, thus acting as the central backbone of the entire assembly.

These two requirements, a metallic nozzle body and mechanical integration into the grounded process chamber, result in a significant technical limitation: An electrically floating configuration of the nozzle, which was identified as optimal in Section 5.1.3, could not be realized under these constraints. Since both the chamber itself and all connected components are electrically grounded. There still remained a possibility to keep the entire chamber floating and electrically decoupled from all diagnostic devices. The realization of this idea, however, required considerable technical effort and posed significant safety risks, as large sections of the system would have been subjected to high voltage.

5.2.1 Experimental Integration into the Levitator Unit

The initial tests (see Figure 5.8 and Chapter 4.3) within the levitation chamber revealed a clear trend: The Plasma ignition was successful, the sample was stably levitated, but no visible jet

emerged from the nozzle. It was clearly observed that the discharge extended up to the nozzle outlet but ended abruptly at that point.

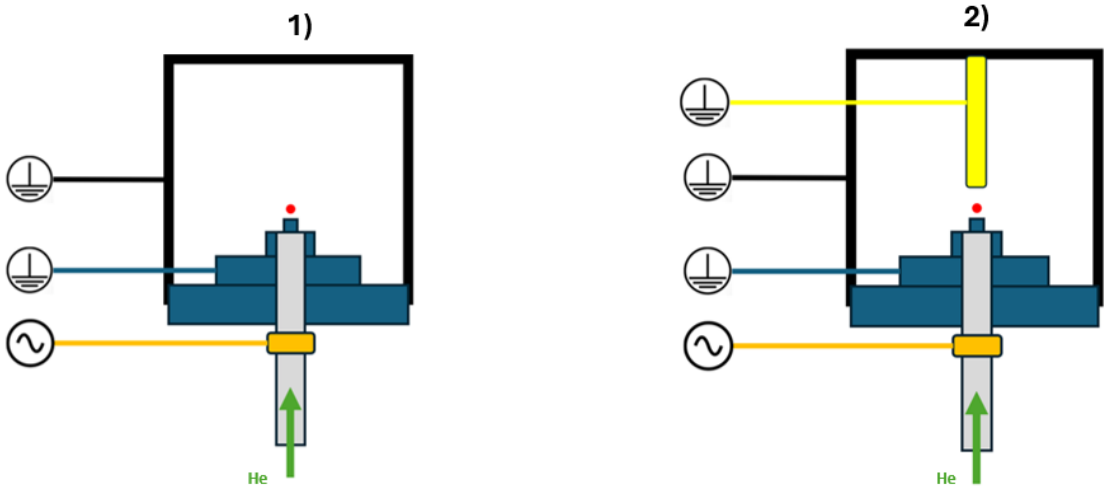

Figure 5.8: Schematic representation of the two coupling tests. (1) Initial configuration with grounded nozzle body. (2) Extension by an additional rod electrode to provoke plasma jet formation despite the grounded nozzle body.

A serendipitous observation occurred during the removal of the levitated sample using a metallic, grounded tweezer. As the tweezer approached the nozzle outlet, it visibly pulled the discharge out of the nozzle. This observation led to the hypothesis that a deliberately placed, grounded counter-electrode at the nozzle exit might enable stable plasma jet formation even with the nozzle grounded.

To verify this assumption, the initial setup was modified by adding a centrally aligned rod electrode, as shown in Figure 5.8. This electrode was electrically grounded and positioned directly in front of the nozzle outlet.

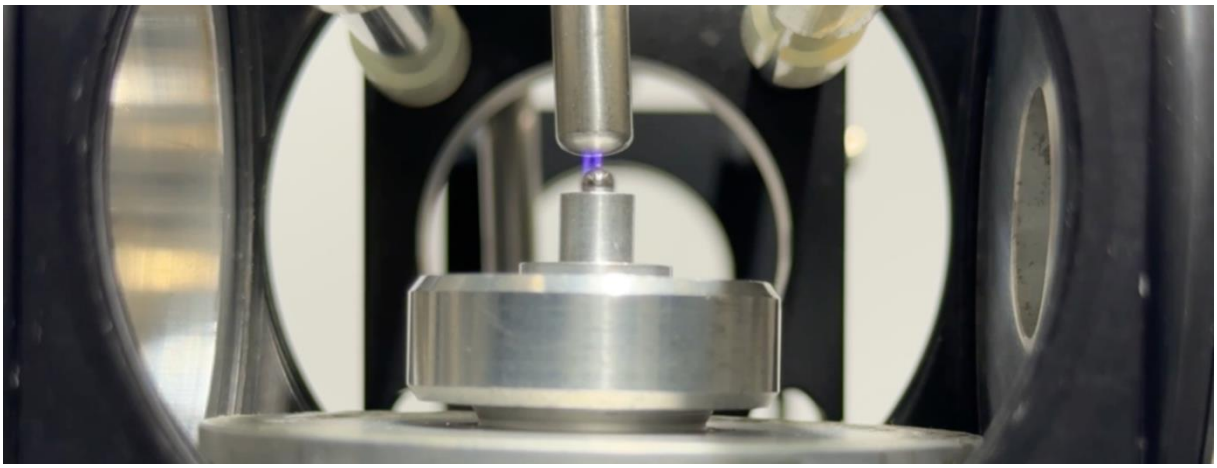

Figure 5.9: Demonstration of simultaneous aerodynamic levitation and plasma operation. A grounded rod electrode is positioned at the nozzle outlet, allowing the plasma to be pulled out of the grounded nozzle. The metallic sample is levitating in the gas stream above the nozzle while interacting with the plasma.

Under these conditions, simultaneous plasma generation and stable levitation were successfully demonstrated for the first time. The plasma visibly emerged from the nozzle and reached the levitated sphere, enabling direct interaction between the plasma and the sample surface (see Fig. 5.9).

Despite this successful demonstration of combined plasma and levitation operation, the configuration introduced significant limitations. The use of an external counter-electrode at the nozzle exit prevented the simultaneous operation of both CO_2 lasers. The lower laser beam would directly strike the metallic electrode, causing substantial heating, while the confined space within the diagnostics module made alternative routing of the upper laser infeasible.

Furthermore, this setup did not align with the intended reactor design. The goal was to develop a compact, integrated system in which the plasma unit could be permanently coupled to the levitation nozzle without the need for external components such as additional electrodes. The use of a separate ground electrode thus served only as an experimental proof of concept and was not pursued further in the final reactor configuration

5.2.2 Operation of the Reactor with Modified Nozzle Body

It became evident that electrical isolation needed to be applied specifically to the nozzle, while the rest of the nozzle body had to remain electrically decoupled from the overall system. This required the use of an electrically non-conductive nozzle body, since the process chamber had to remain unchanged to ensure compatibility with existing components such as the laser units, diagnostic systems and levitation module.

A key limitation was imposed by the lower CO_2 laser, which had been used in earlier levitation tests to avoid vertical temperature gradients. Since the process gas enters the chamber from below, the underside of the sample is subjected to convective cooling. Without bottom-side heating, this leads to asymmetric temperature distributions. However, for the reduction experiments conducted in this work, this effect was not considered to be-critical. As a result, the lower laser was omitted from the prospective design.

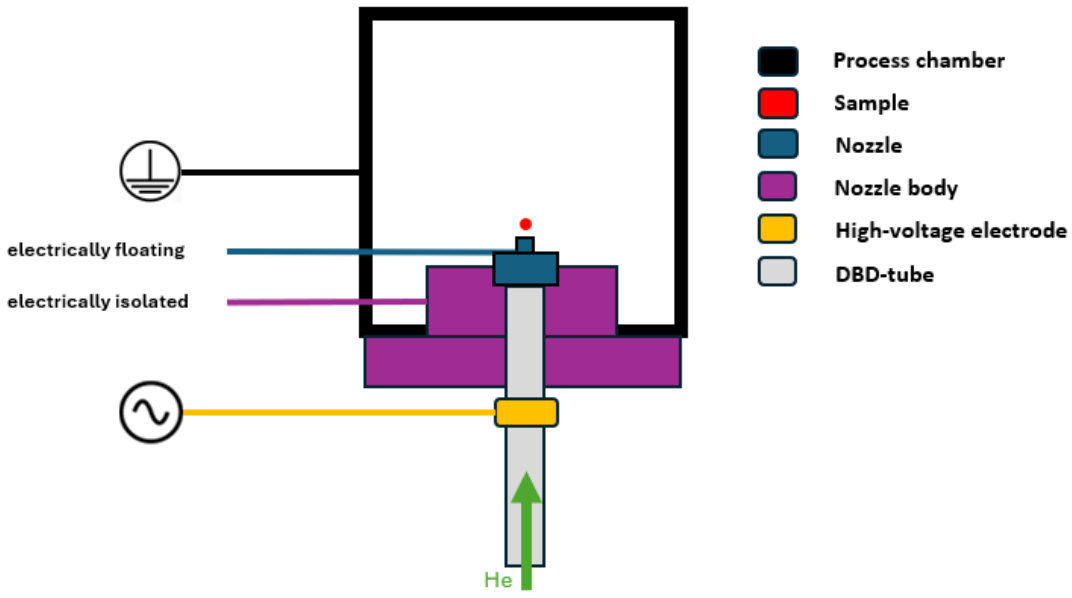

Figure 5.10: Schematic representation of the prototype with electrically insulated nozzle body.

This decision made it possible to manufacture the entire nozzle body from an electrically insulating material. A new nozzle body (Figure 4.12) was designed. It consisted entirely of PLA, except for the metallic nozzle and a few mounting screws. The component was fabricated

using additive manufacturing. The high-voltage electrode was mounted on the outer surface of the quartz tube.

Using this newly designed system (Figure 5.10), the experiment was repeated. As illustrated in Figure 5.11, a stable plasma jet emerged from the nozzle without the need for an external counter-electrode. At the same time, the sample remained stably levitated in the gas stream. This result confirms that the use of a floating nozzle body allows simultaneous operation of the plasma jet and aerodynamic levitation.

The tested configuration serves as the basis for the final reactor design described in Chapter 5.3. In the right image of Figure 5.11, additional plasma structures can be observed below the nozzle. These resulted from gas leakage between the metallic nozzle and the PLA body. Since the transition area between both parts was not fully sealed in this prototype, helium escaped through the gap. To enhance the visibility of the plasma jet and the levitated sphere, the gas flow was increased up to 2 L/min. This higher flow rate intensified the leakage effect. In the final design, the gas channel will be properly sealed to eliminate this issue.

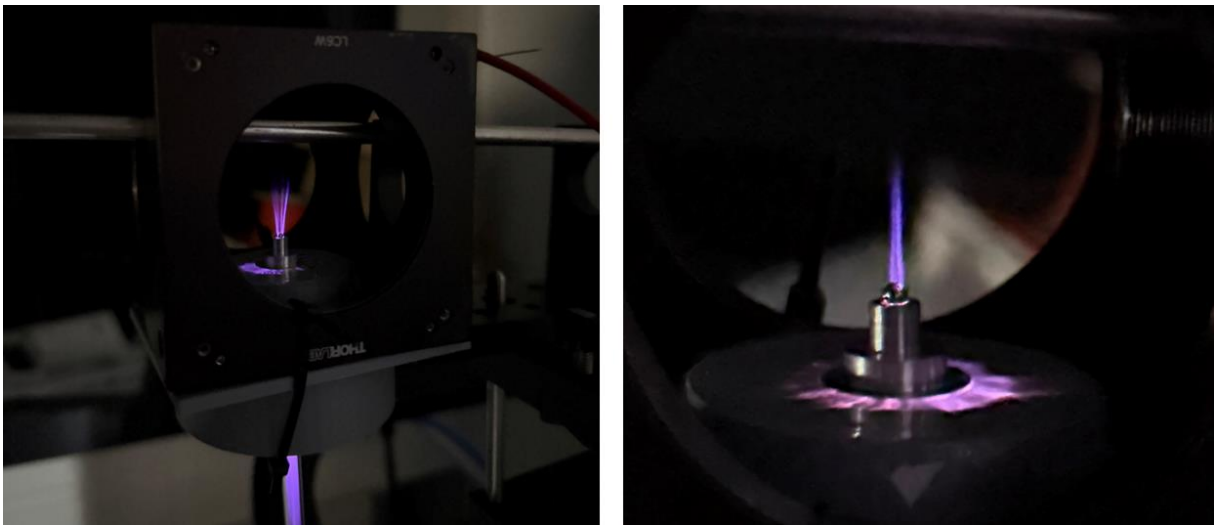

Figure 5.11: Successful demonstration of combined levitation and plasma jet using an additively manufactured nozzle body. The quartz tube with embedded HV electrode is integrated into the insulating structure, while the metallic nozzle is mounted on top. The plasma jet emerges clearly from the nozzle and reaches the levitated sphere, enabling simultaneous operation of plasma and levitation with only one electrode.

5.3 Development of the Final Reactor Design

The experimental investigations presented in the previous sections provided essential insights that directly guided the development of the final reactor configuration. These findings covered a wide range of parameters, including plasma ignition thresholds, gas flow requirements for stable levitation, electrode design, material compatibility, and system-level constraints imposed by the integration with the existing levitation chamber.

Table 5.1: Technical Requirements and Experimental Findings for the Final Reactor Design

Category	Technical Requirements / Experimental Findings
Ignition and Operating Parameters	- Stable levitation achieved at ≥ 0.4 L/min gas flow rate - Process gas: Helium with 3% hydrogen - Plasma ignition at 17 kVpp and 5 kHz - Stable discharge at 11 kHz
System-Level Constraints	- Process chamber must remain unchanged (integration of laser, diagnostics, levitation module) - Only top-side laser allowed - Optical access required for diagnostics - Significant thermal load due to laser heating
Material and Component Selection	- Nozzle must be metallic (thermal durability, heat dissipation) - Nozzle body must be electrically insulating - Electrode must be conductive and have no sharp edges - Dielectric barrier required for discharge stabilization

Table 5.1 summarizes the most relevant technical findings and boundary conditions identified throughout the test. These results form the foundation upon which the following design decisions were based.

5.3.1 Final Reactor Design

The final reactor design builds upon the experimental setup presented in Section 5.2.2 but was systematically refined based on the insights gained during the preceding test campaigns. The fundamental structure of the reactor is illustrated in Figure 5.12.

Figure 5.12: Assembly of the final reactor system including process chamber, nozzle unit, integrated water cooling, and embedded electrode. The right-hand side shows an exploded view of the reactor system

The optical cube from Thorlabs serves as a process chamber. The four lateral ports of the cube match the interface diameters of the existing levitation system, which allows all diagnostic components such as the camera, pyrometer, and mirrors to be reused without mechanical modifications. Only the top and bottom openings of the cube are slightly enlarged. This design

feature proves beneficial for integrating the larger, water-cooled nozzle assembly. Since most of the components are standardized Thorlabs parts, only the upper end cap, previously housing the laser and pyrometer, had to be modified and reordered. A technical drawing of the chamber cube is included in the appendix.

The embedded high-voltage electrode used in the reactor was developed and optimized specifically during the test campaigns. Its geometry allows for a rapid replacement of the high-voltage cable in the event of mechanical failure or electrical disconnection. To prevent unintended discharges, the electrode is fully enclosed within the nozzle body, providing complete electrical insulation. This design ensures that no arcs can form between the electrode and nearby conductive structures and eliminates the risk of accidental contact with operating personnel.

As a dielectric barrier, a quartz glass tube is used once more. Owing to its high dielectric strength, thermal stability, and chemical resistance, quartz is ideally suited for dielectric barrier discharge (DBD) applications. The tube's length can be easily adjusted to fit different geometries. To prevent gas leaks, which were observed in earlier tests, an O-ring seal is integrated between the nozzle and the nozzle body in the final design. This ensures both gas-tight sealing and mechanical stabilization of the plasma channel (see Figure 5.13).

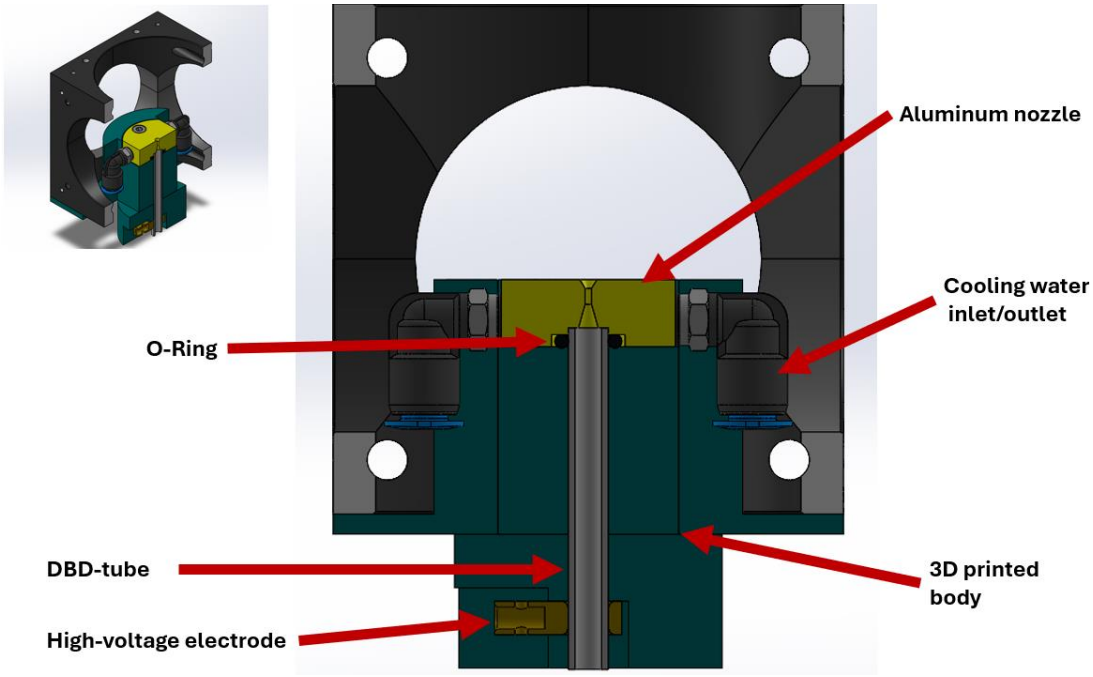

Figure 5.13: Detailed view of the nozzle unit with integrated O-ring seal for gas-tight connection between the metallic nozzle and the nozzle body. The quartz tube is axially inserted into the nozzle body and the high-voltage electrode is mounted on it.

The core component of the reactor is the metallic nozzle, which is fabricated, out of aluminum. The Laval geometry that defines the gas flow through the nozzle was directly adopted from the validated levitation setup to ensure stable aerodynamic conditions. Aluminum was chosen for its high thermal conductivity and ability to effectively reflect the CO_2 laser's radiation, thereby minimizing unwanted heating of the insulating nozzle body. Compared to the original levitator nozzle, the plasma nozzle is significantly larger (see Figure 5.14). This enlargement serves two purposes. First, it ensures a sufficient spatial separation between the laser beam and the insulating body. Second, it provides the necessary space to integrate a water cooling system. Two parallel cooling channels were added near the nozzle exit. Water enters from one side

and exits on the opposite side, enabling efficient heat removal from both laser and plasma-induced thermal loads. The increased nozzle dimensions required the use of the larger Thorlabs cube to accommodate the necessary installation height.

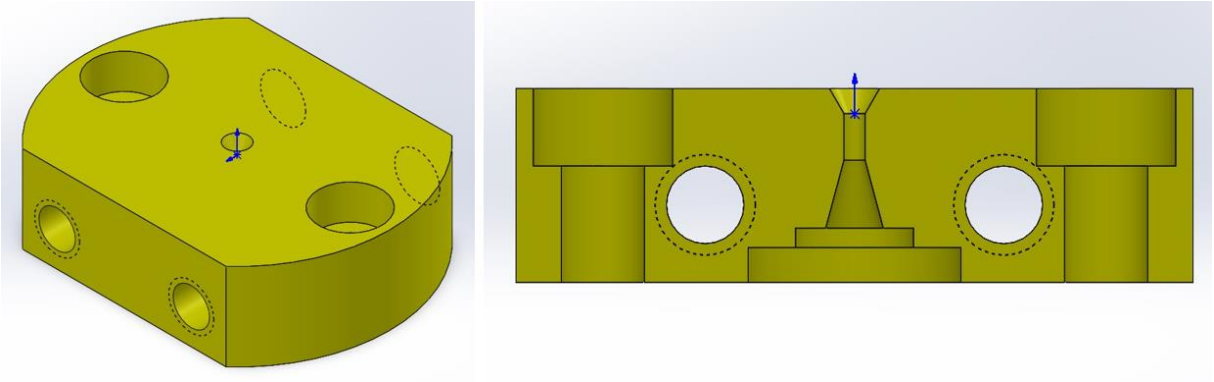

Figure 5.14: CAD model of the nozzle with dimensions of 10 mm in height, 26 mm in width, and 35 mm in length. The right image shows the cross-section, revealing the Laval contour and the two integrated cooling channels.

The nozzle is mechanically attached to the rest of the nozzle body using two M4 countersunk screws. These screws ensure stable mechanical fixation and generate the pressure necessary for sealing the O-ring. The entire nozzle body is composed of two separate parts, manufactured via additive fabrication from polyamide (PA). This material offers a favorable combination of mechanical strength, thermal stability, and electrical insulation properties. The lower part houses the electrode and enables quick removal from the underside of the reactor. The upper part supports the nozzle and ensures that no electrical contact occurs between the electrically floating aluminum nozzle and the grounded chamber walls. This isolation is essential for maintaining the potential difference required for stable DBD operation. The upper part is for mechanically attaches the entire nozzle module to the chamber.

The final configuration fulfills all functional requirements for plasma generation, aerodynamic levitation, thermal robustness, and electrical safety while maintaining a modular architecture that is compatible with the existing experimental infrastructure

5.3.2 Limitation of this Work

Despite the successful development and implementation of a functional reactor system that combines aerodynamic levitation with DBD plasma operation, several limitations remain that could not be fully addressed within the scope of this thesis.

A central issue concerns the final commissioning of the complete reactor system. While the individual subsystems were validated through the experiments presented in Chapter 4, demonstrating both stable levitation and a directed plasma jet, the full integration into the existing levitation platform could not be completed. Due to the extended fabrication time of the manufactured components, it was not possible to assemble and test the entire reactor unit within the available timeframe. As a result, no final alignment of the diagnostic and optical systems in the operational setup could be performed.

This also affected the experimental validation of the water-cooling system. Although the aluminum nozzle was equipped with integrated cooling channels and included in the final

reactor design, its thermal performance under real CO_2 laser conditions was not evaluated. Furthermore, the electrical influence of the cooling water on the plasma behavior was not tested directly but estimated theoretically. Based on this assessment, at a given frequency the cooling water will not be in an electrical contact with the aluminum nozzle due to the skin effect.

An important limitation of this work is that the developed setup was never operated continuously for more than five minutes. The focus of the experiments was on demonstrating the basic functionality of the system and obtaining the results defined within the scope of this thesis. Consequently, no reliable data are available regarding the plasma behavior during extended operation. In particular, it remains unclear whether the system maintains thermal stability and whether integration of the electrode into an active cooling circuit would be necessary. Furthermore, no instrumental temperature measurements were carried out. However, the short test runs clearly demonstrated that the discharge corresponds to a cold atmospheric plasma, as it could be safely touched by hand without thermal load.

Another limitation relates to the process gas composition. While the intended application involves a helium-hydrogen mixture for oxide reduction experiments, all tests conducted in this work were limited to pure helium. The helium-hydrogen mixture was not available at the time of testing, meaning that the ignition behavior, plasma stability, and general discharge parameters were characterized solely for helium. The effect of hydrogen admixture on plasma ignition remains unaddressed.

Despite these limitations, the developed system provides a robust foundation for future investigations. The documented design strategies, functional results, and technical insights offer a solid basis for continued research on plasma-assisted levitation for high-temperature material processing.

6 Conclusion

The primary objective of this thesis was to develop a reactor system that combines aerodynamic levitation (ADL) with a dielectric barrier discharge (DBD) plasma at atmospheric pressure. The goal was to create an experimental platform that allows for containerless stabilization and simultaneous plasma treatment of mm-sized samples. A central requirement was the ability to independently control the thermal and plasma-related parameters, enabling detailed investigation of surface reactions in high-temperature materials.

To achieve this, a modular reactor was designed, constructed and experimentally validated. The system consists of a newly developed nozzle body with integrated water cooling and electrical insulation. It was tailored to match the geometrical and functional requirements of the existing ADL setup. The plasma was operated using helium as the process gas and produced a stable, directed jet that could be coupled into the levitation zone without affecting the aerodynamic stability

System commissioning was carried out in two successive stages. In the first configuration, a grounded electrode at the nozzle outlet enabled extraction of the plasma jet toward the levitated sample. Stable levitation and visible plasma interaction were successfully demonstrated. In the second stage, a fully insulated nozzle holder made of polymer was developed to support a water-cooled metallic nozzle. This version integrated the plasma feed, gas routing and electrode connection into a compact unit. The positive results from both setups provided the functional basis for the final reactor design.

The results show that the simultaneous operation of plasma and levitation is technically feasible. The reactor enables interaction between a cold atmospheric plasma and a free-floating sample. With the successful demonstration of plasma ignition, stable levitation and sample exposure, the main goal of this thesis has been achieved. A functional and modular platform was created that expands the experimental possibilities for containerless surface processing.

Based on the results, several directions for future research can be identified. First, the complete integration of the final reactor into the existing ADL system should be implemented. This includes alignment of optical components, laser beam paths and diagnostics within the closed process chamber. Only under these conditions can the system be validated for routine experiments with full process control.

Second, the influence of the internal water-cooling loop on the electric field distribution of the plasma should be examined experimentally. Although theoretical estimates suggest minimal interaction, verification under real operating conditions is essential, especially in the presence of thermal gradients introduced by the laser.

Third, the use of helium-hydrogen mixtures should be explored to assess the behavior of the plasma under chemically reactive conditions. The addition of hydrogen could increase the formation of reactive species while maintaining plasma stability. This would allow targeted studies of the ignition behavior and chemistry of plasma jets in reducing environments.

Fourth, the system offers the opportunity to study redox reactions under conditions where plasma and temperature effects are independently controlled. Through selective adjustment

of the plasma input and laser heating, it is possible to determine whether material transformations are triggered thermally, plasma chemically or by a combination of both factors. This could help to clarify the mechanisms of oxide reduction in plasma-supported environments.

References

[1] M. Laroussi *et al.,* "Low Temperature Plasma for Biology, Hygiene, and Medicine: Perspective and Roadmap," 2021. [Online]. Available: https://arxiv.org/pdf/2108.03158

[2] P. Gibbon, "Introduction to Plasma Physics," 2016, doi: 10.5170/CERN-2016-001.51.

[3] I. Adamovich *et al.,* "The 2022 Plasma Roadmap: low temperature plasma science and technology," *J. Phys. D: Appl. Phys.*, vol. 55, no. 37, p. 373001, 2022, doi: 10.1088/1361-6463/ac5e1c.

[4] A. Pack, K. Kremer, N. Albrecht, K. Simon, and A. Kronz, "Description of an aerodynamic levitation apparatus with applications in Earth sciences," *Geochemical transactions*, vol. 11, p. 4, 2010, doi: 10.1186/1467-4866-11-4.

[5] Y. Suenaga *et al.,* "Influence of Controlling Plasma Gas Species and Temperature on Reactive Species and Bactericidal Effect of the Plasma," *Applied Sciences*, vol. 11, no. 24, p. 11674, 2021, doi: 10.3390/app112411674.

[6] V. Contreras, R. Valencia, J. Peralta, H. Sobral, M. A. Meneses-Nava, and H. Martinez, "Chemical elemental analysis of single acoustic-levitated water droplets by laser-induced breakdown spectroscopy," *Optics letters*, vol. 43, no. 10, pp. 2260–2263, 2018, doi: 10.1364/OL.43.002260.

[7] C. Poulain, A. Dugué, A. Durieux, N. Sadeghi, and J. Duplat, "The plasma levitation of droplets," *Applied Physics Letters*, vol. 107, no. 6, 2015, doi: 10.1063/1.4926964.

[8] P. Snabre, M. Announ, J. M. Badie, and B. Granier, "Heat transfer around a spherical particle levitated in argon plasma jet," *Eur. Phys. J. AP*, vol. 3, no. 3, pp. 287–293, 1998, doi: 10.1051/epjap:1998232.

[9] C. J. Benmore and J. K. R. Weber, "Aerodynamic levitation, supercooled liquids and glass formation," *Advances in Physics: X*, vol. 2, no. 3, pp. 717–736, 2017, doi: 10.1080/23746149.2017.1357498.

[10] Y. Gong, L. Zhang, Y. Yuan, and W. Ma, "Non-Contact Thermophysical Property Measurements of High-Temperature Corium Through Aerodynamic Levitation," *Energies*, vol. 18, no. 1, p. 136, 2025, doi: 10.3390/en18010136.

[11] Y. Gong, L. Zhang, Y. Yuan, Q. Guo, W. Ma, and S. Huang, "Density Measurement of Molten Drop With Aerodynamic Levitation and Laser Heating," *Front. Energy Res.*, vol. 10, 2022, doi: 10.3389/fenrg.2022.892406.

[12] D. R. Neuville, L. Hennet, P. Florian, and D. de Ligny, "In situ High-Temperature Experiments," *Reviews in Mineralogy and Geochemistry*, vol. 78, no. 1, pp. 779–800, 2014, doi: 10.2138/rmg.2013.78.19.

[13] S. Shimizu *et al.,* "The approach to diamond growth on levitating seed particles," *Applied Surface Science*, vol. 254, no. 1, pp. 177–180, 2007, doi: 10.1016/j.apsusc.2007.07.017.

[14] G. Praburam and J. Goree, "A new plasma method of synthesizing aerosol particles," *Journal of Aerosol Science*, vol. 27, no. 8, pp. 1257–1268, 1996, doi: 10.1016/0021-8502(96)00020-1.

[15] E. W. Leung and K. F. Man, "Plasma heating for containerless and microgravity materials processing," Patent Number: US-PATENT-5,374,801, Dec. 1994. [Online]. Available: https://ntrs.nasa.gov/citations/19950011911

[16] V. Udachin, L. Wegewitz, M. Szafarska, S. Dahle, R. Gustus, and W. Maus-Friedrichs, "Atmospheric Non-thermal Plasma Reduction of Natively Oxidized Iron Surfaces," *Plasma Chem Plasma Process*, vol. 43, no. 5, pp. 957–974, 2023, doi: 10.1007/s11090-023-10346-7.

[17] S. Kumar, Z. Xiong, J. Held, P. Bruggeman, and U. R. Kortshagen, "Rapid carbon-free iron ore reduction using an atmospheric pressure hydrogen microwave plasma," *Chemical Engineering Journal*, vol. 472, p. 145025, 2023, doi: 10.1016/j.cej.2023.145025.
[18] D. S. Ellis *et al.,* "Understanding the Contribution of Surface Temperature and Hydrogen Radicals to Hydrogen Plasma Reduction of Iron Oxide," *ACS Sustainable Chem. Eng.*, vol. 13, no. 21, pp. 7760–7768, 2025, doi: 10.1021/acssuschemeng.5c00559.
[19] J. Kim *et al.,* "Decarbonizing the iron and steel industry: A systematic review of sociotechnical systems, technological innovations, and policy options," *Energy Research & Social Science*, vol. 89, p. 102565, 2022, doi: 10.1016/j.erss.2022.102565.
[20] A. Zakeri, K. S. Coley, and L. Tafaghodi, "Hydrogen-Based Direct Reduction of Iron Oxides: A Review on the Influence of Impurities," *Sustainability*, vol. 15, no. 17, p. 13047, 2023, doi: 10.3390/su151713047.
[21] Wikipedia, *Levitation (physics).* [Online]. Available: https://en.wikipedia.org/w/index.php?title=Levitation_(physics)&oldid=1308691656 (accessed: Sep. 15 2025).
[22] B. Glorieux, "Aerodynamic levitation: An approach to microgravity," in *AIP Conference Proceedings*, Albuquerque, New Mexico, Feb. 2001, pp. 316–324.
[23] *Electromagnetic Levitator turns ten.* [Online]. Available: https://www.esa.int/Science_Exploration/Human_and_Robotic_Exploration/Electromagnetic_Levitator_turns_ten (accessed: Sep. 11 2025).
[24] M. Mohr *et al.,* "Electromagnetic levitation containerless processing of metallic materials in microgravity: thermophysical properties," *NPJ microgravity*, vol. 9, no. 1, p. 34, 2023, doi: 10.1038/s41526-023-00281-4.
[25] R. W. Hyers and J. R. Rogers, "A Review of Electrostatic Levitation for Materials Research," *High Temperature Materials and Processes*, vol. 27, no. 6, 2008, doi: 10.1515/HTMP.2008.27.6.461.
[26] HowStuffWorks, *How Acoustic Levitation Works.* [Online]. Available: https://science.howstuffworks.com/acoustic-levitation.htm (accessed: Sep. 11 2025).
[27] T. G. Wang, "Acoustic Levitation and Manipulation for Space Applications," in *1979 Ultrasonics Symposium*, Sep. 1979 - Sep. 1979, pp. 471–475.
[28] D. Langstaff, M. Gunn, G. N. Greaves, A. Marsing, and F. Kargl, "Aerodynamic levitator furnace for measuring thermophysical properties of refractory liquids," *Review of Scientific Instruments*, vol. 84, no. 12, p. 124901, 2013, doi: 10.1063/1.4832115.
[29] L. Hennet, D. Holland Moritz, R. Weber, and A. Meyer, "High-Temperature Levitated Materials," in *Experimental Methods in the Physical Sciences, Neutron Scattering - Applications in Biology, Chemistry, and Materials Science*: Elsevier, 2017, pp. 583–636.
[30] Jad KOZAILY, "Structure et dynamique d'aluminosilicates de calcium fondus," Doktorarbeit, INSTITUT LAUE LANGEVIN / CEMHTI, UNIVERSITÉ D'ORLÉANS, 2012.
[31] D. Merche, N. Vandencasteele, and F. Reniers, "Atmospheric plasmas for thin film deposition: A critical review," *Thin Solid Films*, vol. 520, no. 13, pp. 4219–4236, 2012, doi: 10.1016/j.tsf.2012.01.026.
[32] M. Laroussi and X. Lu, "Room-temperature atmospheric pressure plasma plume for biomedical applications," *Applied Physics Letters*, vol. 87, no. 11, 2005, doi: 10.1063/1.2045549.
[33] J. Winter, R. Brandenburg, and K.-D. Weltmann, "Atmospheric pressure plasma jets: an overview of devices and new directions," *Plasma Sources Sci. Technol.*, vol. 24, no. 6, p. 64001, 2015, doi: 10.1088/0963-0252/24/6/064001.

[34] B. Platier, T. Staps, P. Koelman, M. van der Schans, J. Beckers, and W. IJzerman, "Probing Collisional Plasmas with MCRS: Opportunities and Challenges," *Applied Sciences*, vol. 10, no. 12, p. 4331, 2020, doi: 10.3390/app10124331.

[35] D. Gidon, D. B. Graves, and A. Mesbah, "Effective dose delivery in atmospheric pressure plasma jets for plasma medicine: a model predictive control approach," *Plasma Sources Sci. Technol.*, vol. 26, no. 8, p. 85005, 2017, doi: 10.1088/1361-6595/aa7c5d.

[36] S. Nijdam, J. Teunissen, and U. Ebert, "The physics of streamer discharge phenomena," *Plasma Sources Sci. Technol.*, vol. 29, no. 10, p. 103001, 2020, doi: 10.1088/1361-6595/abaa05.

[37] G. A. Mesyats, "Similarity laws for pulsed gas discharges," *PHYS-USP*, vol. 49, no. 10, p. 1045, 2006, doi: 10.1070/PU2006v049n10ABEH006118.

[38] X. Lu and K. Ostrikov, "Guided ionization waves: The physics of repeatability," *Applied Physics Reviews*, vol. 5, no. 3, p. 31102, 2018, doi: 10.1063/1.5031445.

[39] M. Teschke, J. Kedzierski, E. G. Finantu-Dinu, D. Korzec, and J. Engemann, "High-speed photographs of a dielectric barrier atmospheric pressure plasma jet," *IEEE Trans. Plasma Sci.*, vol. 33, no. 2, pp. 310–311, 2005, doi: 10.1109/TPS.2005.845377.

[40] X. Lu, M. Laroussi, and V. Puech, "On atmospheric-pressure non-equilibrium plasma jets and plasma bullets," *Plasma Sources Sci. Technol.*, vol. 21, no. 3, p. 34005, 2012, doi: 10.1088/0963-0252/21/3/034005.

[41] J.-S. Oh, P. M. Bryant, and J. W. Bradley, "Discharge and Plasma Bullet Formation in a Capillary DBD Atmospheric-Pressure Microplasma Jet," *IEEE Trans. Plasma Sci.*, vol. 39, no. 11, pp. 2352–2353, 2011, doi: 10.1109/TPS.2011.2160290.

[42] R. Hackam, "Outdoor HV composite polymeric insulators," *IEEE Trans. Dielect. Electr. Insul.*, vol. 6, no. 5, pp. 557–585, 1999, doi: 10.1109/TDEI.1999.9286745.

[43] Y. Fang, "Aufbau einer aerodynamischen Levitationsanlage und Messung thermophysikalischer Parameter an Al_2O_3," Abschlussarbeit, in Kooperation mit Deutsches Zentrum für Luft- und Raumfahrt (DLR), Köln, Hochschule Coburg, Coburg, 2013. [Online]. Available: Unveröffentlichte Abschlussarbeit, DLR Köln

[44] G. Chen, S. Chen, M. Zhou, W. Feng, W. Gu, and S. Yang, *The preliminary discharging characterization of a novel APGD plume and its application in organic contaminant degradation - IOPscience.* [Online]. Available: https://iopscience.iop.org/article/10.1088/0963-0252/15/4/002 (accessed: Sep. 25 2025).

[45] S. Javanmard and S. G. Pouryoussefi, "Comparison of characteristics of atmospheric pressure plasma jets using argon and helium working gases," *Current Applied Physics*, vol. 46, pp. 61–69, 2023, doi: 10.1016/j.cap.2022.12.002.

Appendix

A: Tables

Table 1: Bill of Materials- Final Reactor

Quantity	Component	Material	Manufacture / Order	Source / Reference
1×	Nozzle	Aluminum	Manufacture	Drawing Appendix B
1×	Nozzle holder	PA (polyamide)	3D print	Drawing Appendix B
1×	Electrode holder	PA (polyamide)	3D print	Drawing Appendix B
1×	High-voltage electrode	Copper	Manufacture	Drawing Appendix B
1×	Process chamber (cube)	Stainless steel / glass (Thorlabs)	Order	Thorlabs SM2C6
1×	DBD quartz tube	Quartz glass, Ø 6 mm outer	Order	G-V-B Shop – D-006-1-0-1500mm EN07
1×	O-ring Ø 6 mm inner	NBR (nitrile butadiene rubber)	Order	Würth- O-Ring 6.00x2.00mm NBR70
4×	Cooling water fitting	Brass / stainless steel	Order	Festo Push-in L-Fitting QSML-M5-6 (festo.com)
2x	Cylinder screw M4 × 45	Stainless steel A2 (ISO 4762 / DIN 912)	Order	Würth – Cylinder screw M4×45 A2-70

Table 2: Technical Information of Polyamid

TECHNICAL INFORMATION

Diameter:	1.75 mm
Diameter Tolerance:	+/- 0.02 mm
Avg Roundness:	+ 0.01 mm
Net Weight:	0.75 kg
Print Temperature:	255°C - 270°C
Bed Temperature:	100°C

Physical Properties	Test Method	Unit	Typical Value
Specific Gravity	ISO 1183	g/cm³	1.01
Mechanical Properties	**Test Method**	**Unit**	**Typical Value**
Tensile Strength @ Yield	ISO 527	MPa	45
Tensile Strength @ Break	ISO 527	MPa	51
Tensile Modulus	ISO 527	MPa	1400
Elongation @ Yield	ISO 527	%	5
Elongation @ Break	ISO 527	%	>200
Flexural Strength	ISO 178	MPa	-
Flexural Modulus	ISO 178	MPa	1150
Izod Impact Strength (Notched) @ 23°C	ISO 180	kJ/m²	12
Thermal Properties	**Test Method**	**Unit**	**Typical Value**
Heat Distortion Temperature @ 0.45 MPa	ISO 75	°C	135
Heat Distortion Temperature @ 1.8 MPa	ISO 75	°C	55
Vicat Softening Temperature	ISO 306	°C	145
Glass Transition Temperature Tg	DSC	°C	-
Melting Temperature Tm	DSC	°C	178
Continuous Use Temperature (UL Yellow Card)	UL 746	°C	65

B: CAD- Drawings

Drawing 1: Electrode

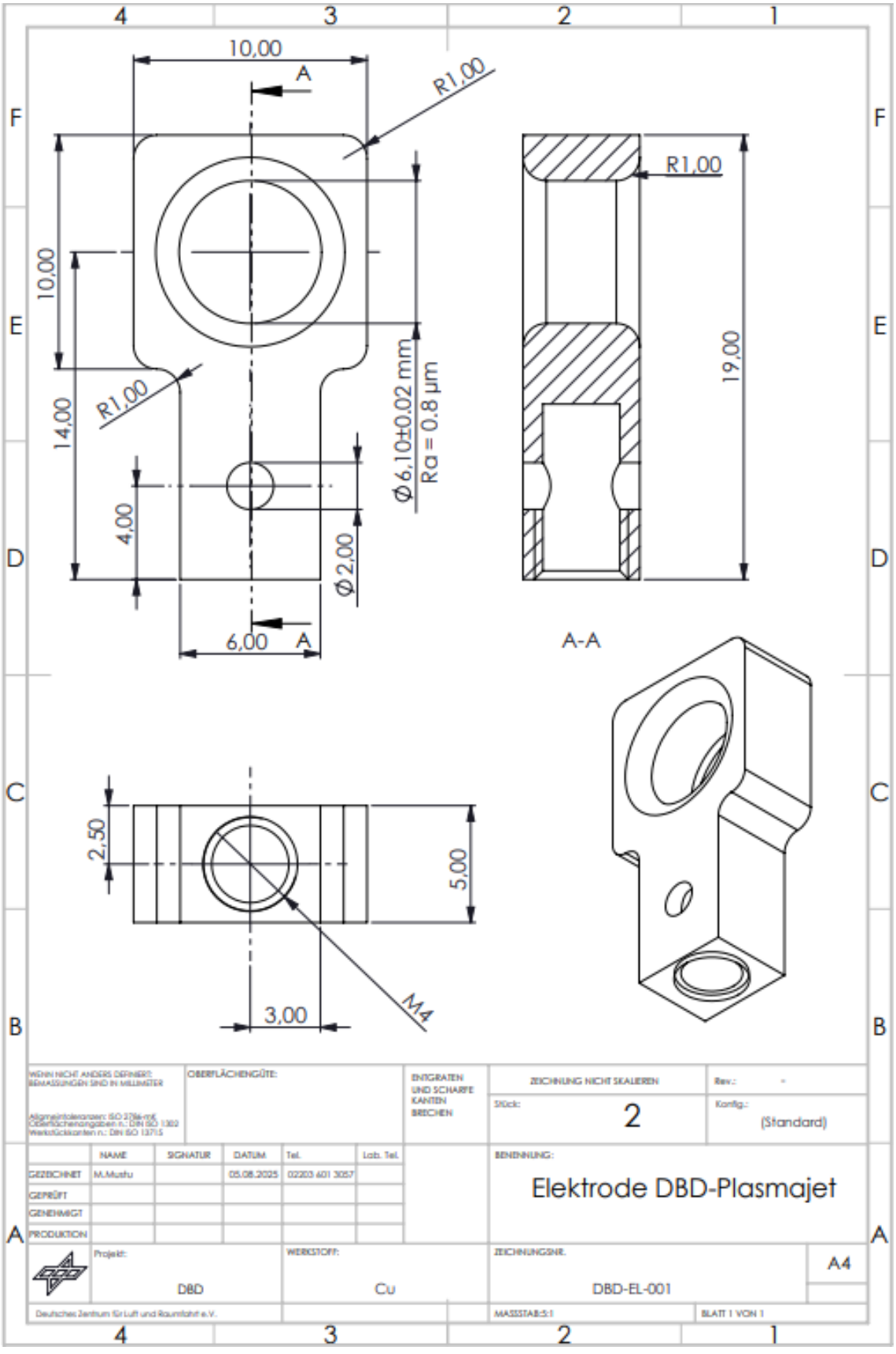

Drawing 2: Nozzle

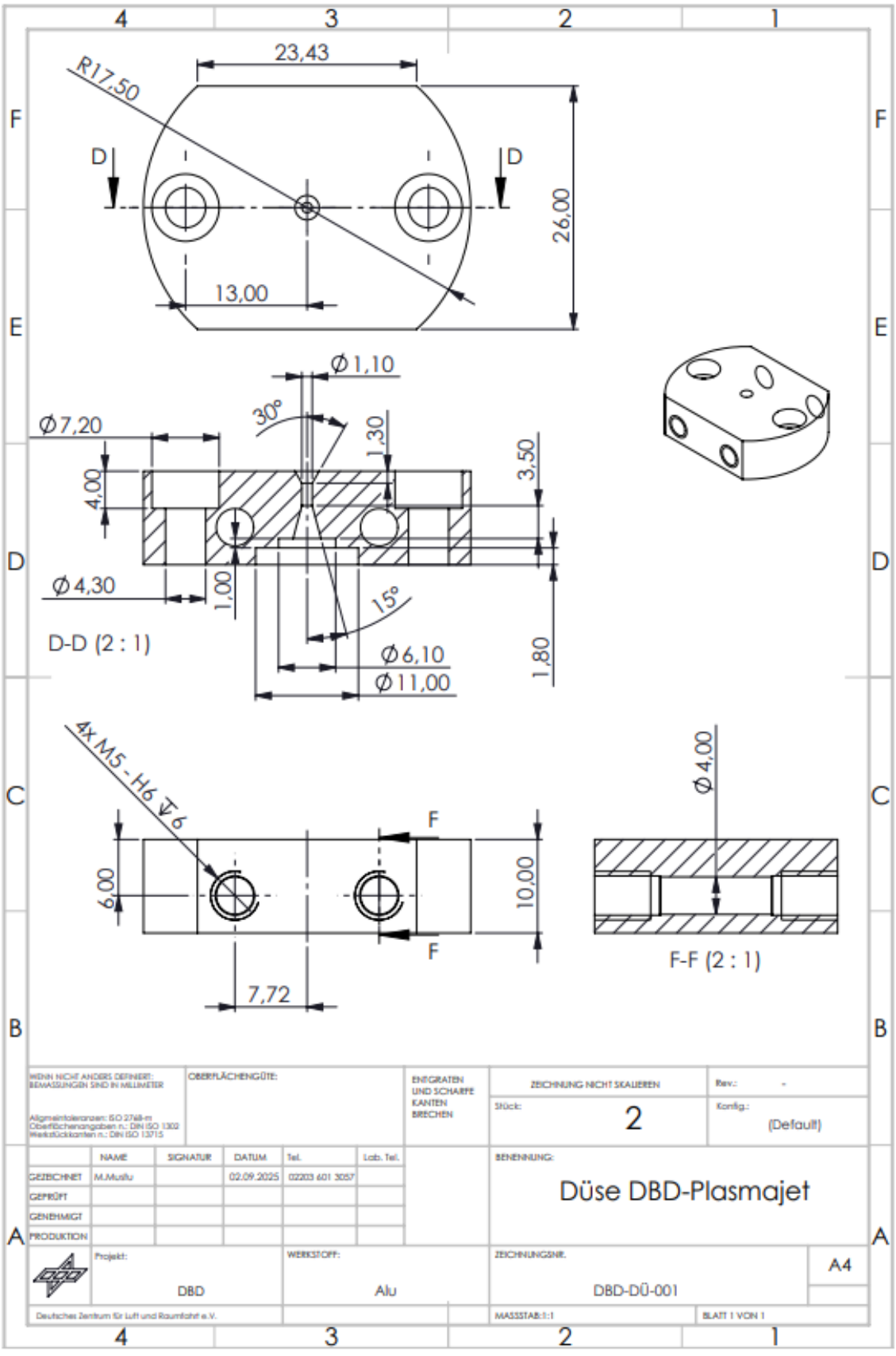

Drawing 3: Nozzle Body

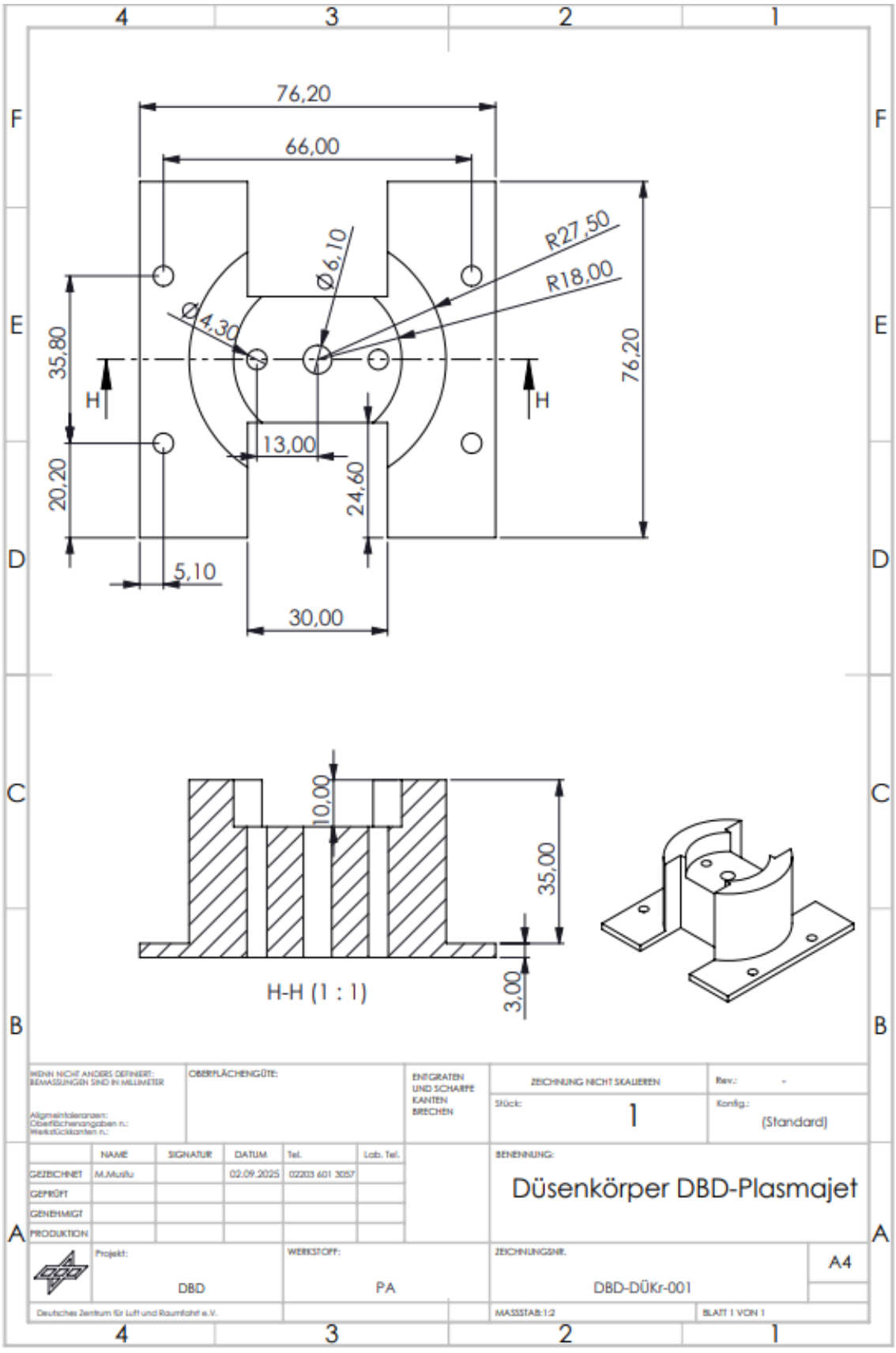

Drawing 3: Electrode Body

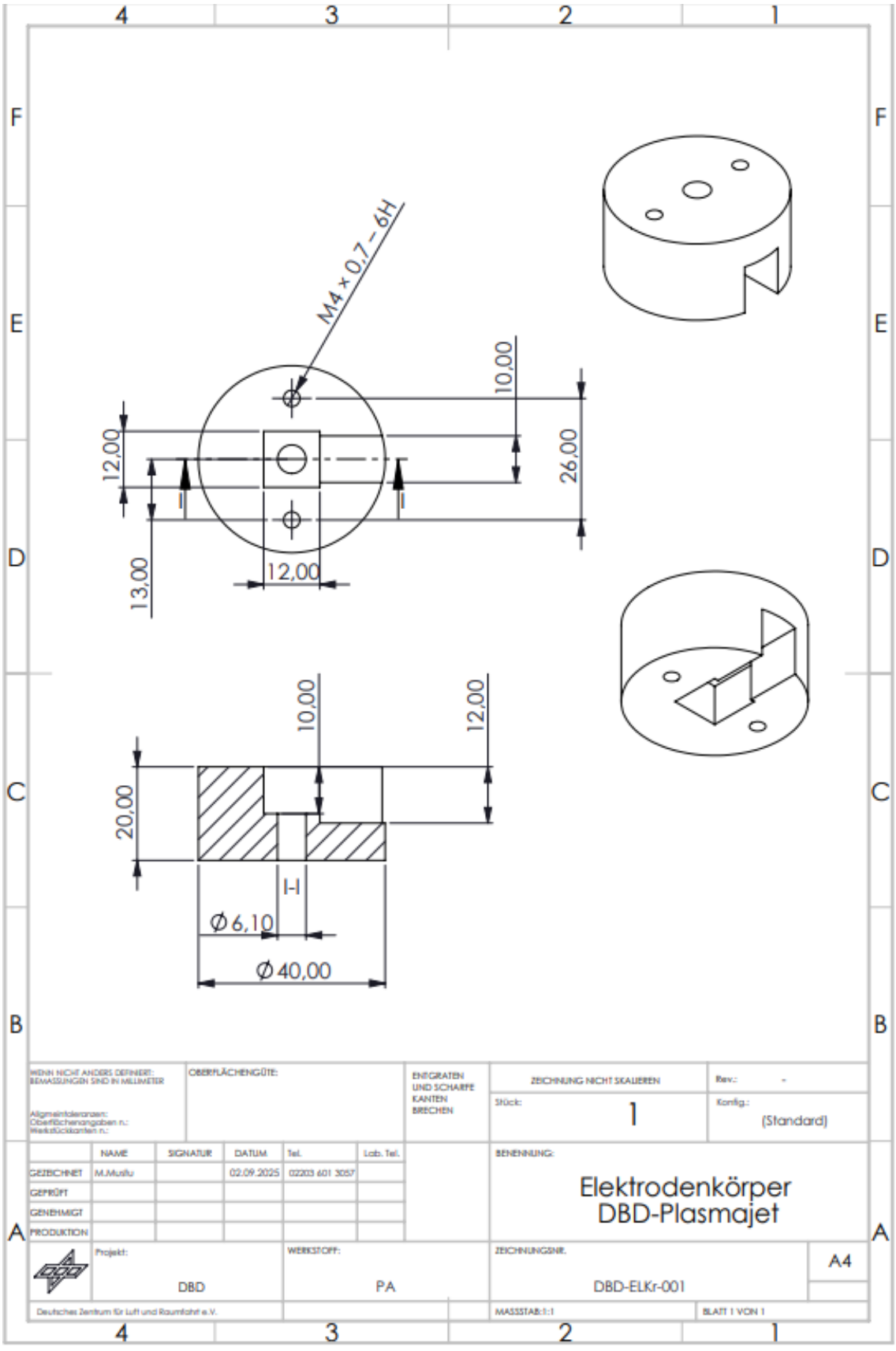

Drawing 4: Assembly of the Reactor

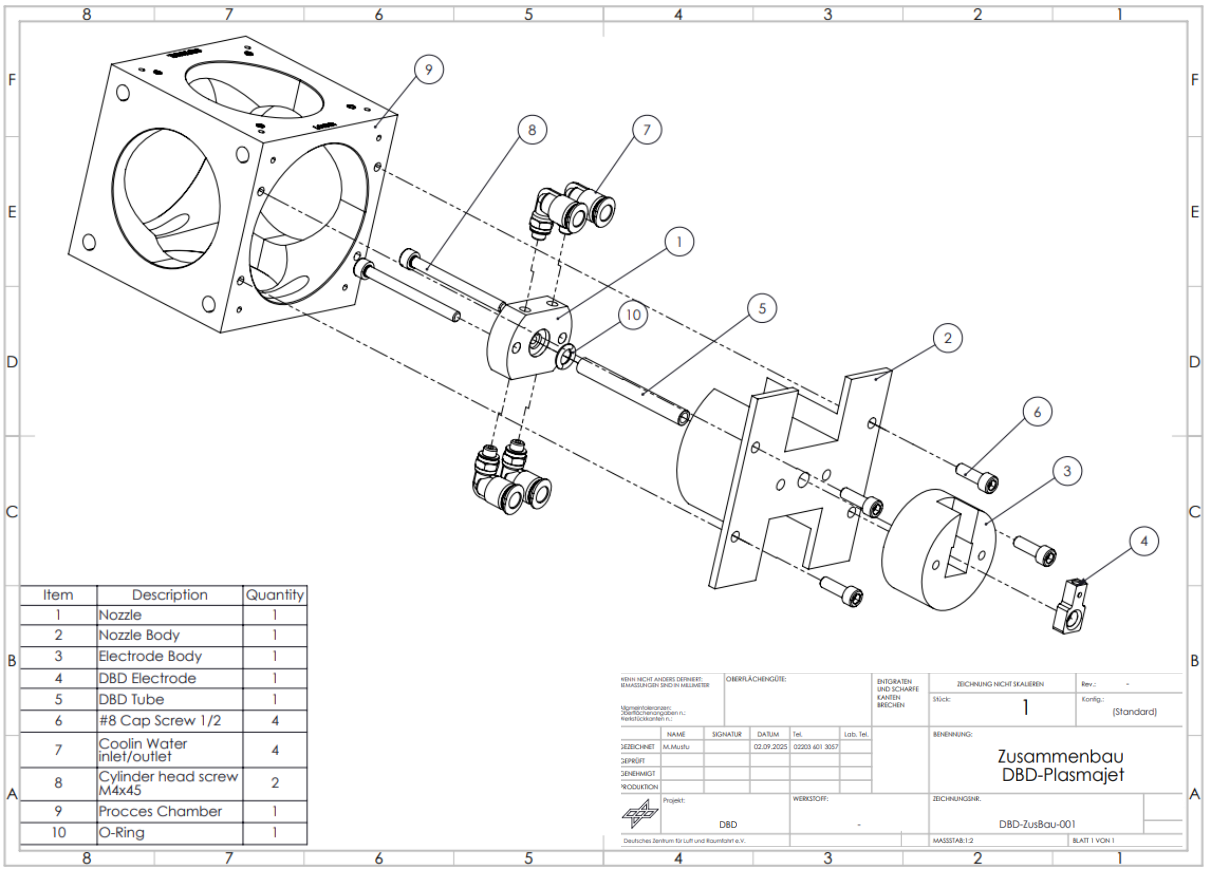

Item	Description	Quantity
1	Nozzle	1
2	Nozzle Body	1
3	Electrode Body	1
4	DBD Electrode	1
5	DBD Tube	1
6	#8 Cap Screw 1/2	4
7	Coolin Water inlet/outlet	4
8	Cylinder head screw M4x45	2
9	Procces Chamber	1
10	O-Ring	1

OBERFLÄCHENGÜTE:				ENTGRATEN UND SCHARFE KANTEN BRECHEN	ZEICHNUNG NICHT SKALIEREN
					Stück: 1
					Rev.: -
					Konfig.: (Standard)
	NAME	SIGNATUR	DATUM	Tel.	Lab. Tel.
GEZEICHNET	M.Mustu		02.09.2025	02203 601 3057	
GEPRÜFT					
GENEHMIGT					
PRODUKTION					

BENENNUNG: Zusammenbau DBD-Plasmajet

Projekt: DBD

WERKSTOFF: -

ZEICHNUNGSNR.: DBD-ZusBau-001

Deutsches Zentrum für Luft und Raumfahrt e.V.

MASSSTAB:1:2 BLATT 1 VON 1